J Neurophysiol 115: 2615–2634, 2016.
First published February 10, 2016; doi:10.1152/jn.00494.2015.

Ca^{2+} removal by the plasma membrane Ca^{2+}-ATPase influences the contribution of mitochondria to activity-dependent Ca^{2+} dynamics in *Aplysia* neuroendocrine cells

Christopher J. Groten, Jonathan T. Rebane, Heather M. Hodgson, Alamjeet K. Chauhan, Gunnar Blohm, and Neil S. Magoski

Department of Biomedical and Molecular Sciences, Physiology Graduate Program, Queen's University, Kingston, Ontario, Canada

Submitted 22 May 2015; accepted in final form 4 February 2016

Groten CJ, Rebane JT, Hodgson HM, Chauhan AK, Blohm G, Magoski NS. Ca^{2+} removal by the plasma membrane Ca^{2+}-ATPase influences the contribution of mitochondria to activity-dependent Ca^{2+} dynamics in *Aplysia* neuroendocrine cells. *J Neurophysiol* 115: 2615–2634, 2016. First published February 10, 2016; doi:10.1152/jn.00494.2015.—After Ca^{2+} influx, mitochondria can sequester Ca^{2+} and subsequently release it back into the cytosol. This form of Ca^{2+}-induced Ca^{2+} release (CICR) prolongs Ca^{2+} signaling and can potentially mediate activity-dependent plasticity. As Ca^{2+} is required for its subsequent release, Ca^{2+} removal systems, like the plasma membrane Ca^{2+}-ATPase (PMCA), could impact CICR. Here we examine such a role for the PMCA in the bag cell neurons of *Aplysia californica*. CICR is triggered in these neurons during an afterdischarge and is implicated in sustaining membrane excitability and peptide secretion. Somatic Ca^{2+} was measured from fura-PE3-loaded cultured bag cell neurons recorded under whole cell voltage clamp. Voltage-gated Ca^{2+} influx was elicited with a 5-Hz, 1-min train, which mimics the fast phase of the afterdischarge. PMCA inhibition with carboxyeosin or extracellular alkalization augmented the effectiveness of Ca^{2+} influx in eliciting mitochondrial CICR. A Ca^{2+} compartment model recapitulated these findings and indicated that disrupting PMCA-dependent Ca^{2+} removal increases CICR by enhancing mitochondrial Ca^{2+} loading. Indeed, carboxyeosin augmented train-evoked mitochondrial Ca^{2+} uptake. Consistent with their role on Ca^{2+} dynamics, cell labeling revealed that the PMCA and mitochondria overlap with Ca^{2+} entry sites. Finally, PMCA-dependent Ca^{2+} extrusion did not impact endoplasmic reticulum-dependent Ca^{2+} removal or release, despite the organelle residing near Ca^{2+} entry sites. Our results demonstrate that Ca^{2+} removal by the PMCA influences the propensity for stimulus-evoked CICR by adjusting the amount of Ca^{2+} available for mitochondrial Ca^{2+} uptake. This study highlights a mechanism by which the PMCA could impact activity-dependent plasticity in the bag cell neurons.

Aplysia californica; Ca^{2+}-induced Ca^{2+} release; neuroendocrine cells; voltage-gated Ca^{2+} channels; Ca^{2+} buffering

INTRACELLULAR CA^{2+} is a fundamental biochemical messenger that controls numerous processes in neurons including transmitter/peptide release, ion channel activity, gene expression, and aerobic metabolism (Berridge 1998; Chouhan et al. 2012; Clapham 2007). Changes to cytosolic Ca^{2+} are derived principally from plasma membrane voltage-gated Ca^{2+} channels but can also be provided by Ca^{2+}-induced Ca^{2+} release (CICR) from intracellular organelles (Berridge 2002). Although CICR has classically been described as arising from the endoplasmic reticulum (ER), an analogous mechanism can also be mediated by the mitochondria and exists in a variety of vertebrate and invertebrate neuronal types (Colegrove et al. 2000a; Friel and Tsien 1994; Geiger and Magoski 2008; Groten et al. 2013; Lee et al. 2007; Tang and Zucker 1997; Werth and Thayer 1994). This process is initiated when Ca^{2+} derived from voltage-gated Ca^{2+} channels diffuses into the mitochondria through a Ca^{2+}-selective ion channel on the inner mitochondrial membrane—the mitochondrial Ca^{2+} uniporter (MCU) (Baughman et al. 2011; Kirichok et al. 2004). Subsequently, Ca^{2+} is slowly released from the mitochondria into the cytosol by a Na^+/Ca^{2+} and/or H^+/Ca^{2+} exchanger (Carafoli et al. 1974; Palty et al. 2010, 2012).

As CICR transduces brief periods of Ca^{2+} influx into prolonged Ca^{2+} signals, it can mediate several forms of activity-dependent plasticity, including posttetanic potentiation of synaptic transmission (Garcia-Chacon et al. 2006; Lee et al. 2007; Tang and Zucker 1997), depolarizing afterpotentials (Partridge and Valenzuela 1999), and afterhyperpolarizations (Davies et al. 1996; Jobling et al. 1993). Considering the significance of these events, it is of central importance to discern the systems that dictate whether a given stimulus will elicit CICR. To date, most research has focused on the role of Ca^{2+} influx through voltage-gated Ca^{2+} channels (Colegrove et al. 2000a, 2000b; D'Arco et al. 2015; Friel and Tsien 1994). Alternatively, the propensity for CICR could be influenced by Ca^{2+} removal systems, such as the plasma membrane Ca^{2+}-ATPase (PMCA) and Na^+/Ca^{2+} exchanger (Clapham 2007). Because Ca^{2+} is required for initiating CICR, these plasma membrane systems, which operate alongside the mitochondria to remove Ca^{2+} from voltage-gated Ca^{2+} channels, would be expected to also impact CICR itself. In the present study, we examined such a role for the PMCA in the bag cell neurons of *Aplysia californica*.

Upon brief stimulation, these neuroendocrine cells undergo a prolonged (~30 min) period of action potential firing called the afterdischarge (Kupfermann 1967; Kupfermann and Kandel 1970). This burst begins with a fast phase of action potential firing (~5 Hz for ~1 min) followed by a slow phase of firing (~1 Hz for ~30 min) (Kaczmarek et al. 1982). During this time, egg-laying hormone is released to initiate the high-priority fixed action pattern of egg laying behavior (Arch 1972; Loechner et al. 1990; Pinsker and Dudek 1977; Wayne et al.

Address for reprint requests and other correspondence: N. S. Magoski, Queen's Univ., Dept. of Biomedical and Molecular Sciences, 4th Floor, Botterell Hall, 18 Stuart St., Kingston, ON, K7L 3N6, Canada (e-mail: magoski@queensu.ca).

1998). Prior work has established that the mitochondria contribute prominently to both Ca^{2+} removal and CICR after voltage-gated Ca^{2+} influx in cultured bag cell neurons (Geiger and Magoski 2008; Groten et al. 2013). Consequently, the mitochondria are implicated in sustaining peptide release and membrane excitability during the afterdischarge (Fisher et al. 1994; Hickey et al. 2010, 2013; Michel and Wayne 2002; Wayne et al. 1998).

Here we demonstrate that, in the presence of an exogenous intracellular Ca^{2+} buffer, Ca^{2+} extrusion by the PMCA limits both the amount of Ca^{2+} taken up by the mitochondria and the ability of Ca^{2+} influx to elicit Ca^{2+} release from this organelle. The influence of the PMCA is specific to mitochondrial Ca^{2+} signaling, as a similar phenomenon does not occur with ER Ca^{2+} uptake or release. This Ca^{2+} interplay could represent a mechanism by which Ca^{2+} removal systems impact activity-dependent Ca^{2+} signaling and possibly neuronal plasticity. For *Aplysia*, our findings suggest that changes in the function and/or expression of the PMCA could impact afterdischarge production and reproductive behavior.

MATERIALS AND METHODS

Animals and Cell Culture

Adult *A. californica* (a hermaphrodite) weighing 150–500 g were obtained from Marinus (Long Beach, CA), housed in an ~300-liter aquarium containing continuously circulating, aerated seawater (Instant Ocean; Aquarium Systems, Mentor, OH) at 14–16°C on a 12:12-h light-dark cycle, and fed romaine lettuce five times per week. All experiments were approved by the Queen's University Animal Care Committee (Protocols Magoski-100323 and Magoski-100845). For primary cultures of isolated bag cell neurons, animals were anesthetized by an injection of isotonic $MgCl_2$ (~50% of body wt) and the abdominal ganglion was removed and treated with Dispase II (13.3 mg/ml; 165859, Roche Diagnostics, Indianapolis, IN) dissolved in tissue culture artificial seawater (tcASW) [composition in mM: 460 NaCl, 10.4 KCl, 11 $CaCl_2$, 55 $MgCl_2$, and 15 *N*-2-hydroxyethylpiperazine-*N*′-2-ethanesulfonic acid (HEPES), with 1 mg/ml glucose, 100 U/ml penicillin, and 0.1 mg/ml streptomycin, pH 7.8 with NaOH] for 18 h at 22°C. The ganglion was then rinsed in tcASW for 1 h, and the bag cell neuron clusters were dissected from their surrounding connective tissue. With the use of a fire-polished glass Pasteur pipette and gentle trituration, neurons were dissociated and dispersed in tcASW onto 35 × 10-mm polystyrene tissue culture dishes (353001, Falcon Becton-Dickinson, Franklin Lakes, NJ). Cultures were maintained in a 14°C incubator in tcASW and used for experimentation within 1–3 days. Salts were obtained from Fisher Scientific (Ottawa, ON, Canada) or Sigma-Aldrich (St. Louis, MO).

Whole Cell Voltage-Clamp Recording

Voltage-clamp recordings were made with an EPC-8 amplifier (HEKA Electronics, Mahone Bay, NS, Canada) and the tight-seal whole cell method. Microelectrodes were pulled from 1.5-mm-external-diameter, 1.2-mm-internal-diameter borosilicate glass capillaries (TW150F-4, World Precision Instruments, Sarasota, FL) and had a resistance of 1–2 MΩ when filled with intracellular saline (see below). For recording pipette junction potentials were nulled, and subsequent to seal formation pipette capacitive currents were canceled and the series resistance (2–5 MΩ) was compensated to 70–80% while the neuronal capacitance current was canceled. Current was filtered at 1 kHz by the EPC-8 built-in Bessel filter and sampled at 2 kHz with an IBM-compatible personal computer and a Digidata 1322A analog-to-digital converter and the Clampex acquisition program of pCLAMP software (v10.2, Molecular Devices, Sunnyvale, CA). Clampex was also used to set the holding and command potentials. Recordings were performed in Ca^{2+}-Cs^{+}-tetraethylammonium (TEA) ASW, as per tcASW but with the NaCl and KCl replaced by TEA-Cl and CsCl, respectively, and the glucose and antibiotics omitted (composition in mM: 460 TEA-Cl, 10.4 CsCl, 55 $MgCl_2$, 11 $CaCl_2$, 15 HEPES, pH 7.8 with CsOH). In some cases, the Ca-Cs-TEA external solution was alkalized with CsOH to produce a high-pH external solution (pH 8.8). Whole cell recordings used a Cs^{+}-aspartate-based intracellular saline [composition in mM: 70 CsCl, 10 HEPES, 11 glucose, 10 glutathione, 5 ethylene glycol-bis(β-aminoethyl ether)-*N,N,N′,N′*-tetraacetic acid (EGTA), 500 aspartic acid, 5 adenosine 5′-triphosphate $2Na{\cdot}H_2O$ (ATP; A3377, Sigma-Aldrich), and 0.1 guanosine 5′-triphosphate $Na{\cdot}H_2O$ (GTP; G8877, Sigma-Aldrich), pH 7.3 with CsOH]. In one set of recordings, EGTA was excluded from the intracellular solution. To image Ca^{2+} (see *Calcium Imaging*) under whole cell voltage clamp, the intracellular saline was supplemented with 1 mM fura-PE3 (0110, TEFLabs, Austin, TX).

Calcium Imaging

For Ca^{2+} imaging, 1 mM fura-PE3 was introduced by dialysis via the whole cell pipette during voltage-clamp recordings. Ca^{2+} imaging was performed with a Nikon TS100-F inverted microscope (Nikon, Mississauga, ON, Canada) equipped with a Nikon Plan Fluor ×20 [numerical aperture (NA): 0.5]. The light source was a 75-W Xe arc lamp and a multi-wavelength DeltaRAM V monochromatic illuminator (Photon Technology International, London, ON, Canada) coupled to the microscope with a UV-grade liquid-light guide. Excitation wavelengths were 340 and 380 nm. The excitation illumination was controlled by a shutter, which along with the excitation wavelength was controlled by the computer, a Photon Technology International computer interface, and EasyRatio Pro software (v1.10, Photon Technology International). To allow for continuous image acquisition during experiments, the shutter was left open. Emitted light passed through a 400-nm long-pass dichroic mirror and a 510/40-nm emission barrier filter before being detected by a Photometrics Cool SNAP HQ2 charge-coupled device camera (Photometrics, Tucson, AZ). The ratio of the emission following 340- and 380-nm excitation (340/380) was taken to reflect free intracellular Ca^{2+} (Grynkiewicz et al. 1985) and saved for subsequent analysis. Image acquisition, emitted light sampling, and ratio calculations were performed with EasyRatio Pro. Ca^{2+} measurements were acquired from a somatic region of interest (ROI) at approximately the midpoint of the vertical focal plane and one-half to three-quarters of the cell diameter. Camera gain was maximized, pixel binning was set at 2, and exposure time at each wavelength was fixed to 1 s. For presentation of ratiometric images in Fig. 7*A*, the background noise in the 340-nm channel was eliminated by applying an arbitrary threshold of 250 fluorescence units.

Live-Cell Staining, Immunocytochemistry, and Immunohistochemistry

For all fluorescence microscopy other than Ca^{2+} imaging, bag cell neurons were prepared as described in *Animals and Cell Culture*, with the exception that cells were plated onto glass coverslips (no. 1, 12-542-B, Fisher Scientific) coated with 1 μg/ml poly-L-lysine hydrobromide (mol wt 300,000, P1534-25MG, Sigma-Aldrich) and glued with Sylgard silicone elastomer (SYLG184, World Precision Instruments) to holes drilled out of the bottom of the tissue culture dish. To visualize the mitochondria, cultured cells were stained with 500 nM MitoTracker Red CMXRos (M-7512, Invitrogen, Eugene, OR) in dimethyl sulfoxide (DMSO; BP231, Fisher Scientific) for 30 min and then washed with nASW (composition as per tcASW but with the antibiotics and glucose omitted). Because MitoTracker Red staining was not well preserved in the soma after fixation, mitochondria were imaged in living cells. On the other hand, fixed neurons

were used to determine the ER distribution with immunocytochemistry and a rat monoclonal antibody against the highly conserved ER-retention signal, KDEL (Lys-Asp-Glu-Leu) (Munro and Pelham 1987) (ab50601, Abcam, Cambridge, MA). This antibody has been used successfully for this purpose in a range of animal species, including *Aplysia* (Lyles et al. 2006; O'Sullivan et al. 2012; Pierrot et al. 2013; Veiga-da-Cunha et al. 2010; Zhang and Forscher 2009). Similarly, PMCA immunocytochemistry was also performed on fixed neurons but with a mouse monoclonal antibody against the purified human erythrocyte PMCA (MA3-914, Thermo Scientific). The antibody recognizes an epitope between residues 724 and 783 of the human PMCA. At the amino acid level, this epitope is 70% identical and 93% homologous with a putative *Aplysia* PMCA homolog, which we identified *in silico* from the University of California Santa Cruz Sea Hare Genome Browser (http://genome.ucsc.edu/cgi-bin/hgGateway?hgsid=446561943_I0RJ4dOl771LBFSkiuH95nQ2cXBK&clade=other&org=Sea+hare&db=0).

For immunocytochemistry, culture dishes were first drained of all fluid except for the contents of the glass-bottomed well and new solutions were delivered by Pasteur pipette directly onto the cells. Neurons were then fixed for 25 min with 4% (wt/vol) paraformaldehyde (04042, Fisher Scientific) in 400 mM sucrose-nASW, pH 7.5 with NaOH. They were then permeabilized for 5 min with 0.3% (wt/vol) Triton X-100 (BP151, Fisher Scientific) in fix and washed twice with PBS (composition in mM: 137 NaCl, 2.7 KCl, 4.3 Na_2HPO_4, 1.5 KH_2PO_4, pH 7.0 with NaOH). Neurons were blocked for 60 min in a blocking solution of 5% (vol/vol) goat serum (G9023, Sigma-Aldrich) in PBS. For single-antibody labeling experiments, the primary antibody, either rat anti-KDEL IgG or mouse anti-PMCA IgG, was applied at 1:200 in blocking solution. Neurons were incubated in the primary antibody in the dark for 1 h and subsequently washed four times with PBS. The secondary antibody against either anti-KDEL (goat anti-rat IgG conjugated to Alexa Fluor 488; A-11006, Invitrogen) or anti-PMCA (goat anti-mouse IgG conjugated to Alexa Fluor 594; A-11005, Invitrogen) was applied at 1:200 in blocking solution and incubated in the dark for 2 h. Neurons were then washed four times with PBS, and the wells were filled with mounting solution [26% (wt/vol) glycerol (BP2291, Fisher Scientific), 11% (wt/vol) Mowiol 4-88 (17951, Polysciences, Warrington, PA), and 110 mM Tris, pH 8.5] and covered with a glass coverslip. For double-labeling experiments, cultured neurons were first processed for PMCA immunolabeling as described above. Subsequently, neurons were washed four times with PBS and then processed for ER immunocytochemistry with the KDEL antibody. Neurons were then washed four times with PBS, and the wells were filled with mounting solution and covered with a glass coverslip.

To visualize cultured bag cell neurons with a single label (MitoTracker Red, anti-KDEL, or anti-PMCA), a Quorum Wave FX-X1 spinning disk confocal system (Quorum Technologies, Guelph, ON, Canada) equipped with a $\times$40 (NA = 0.95) objective was used. Excitation light was provided by a laser line, and emitted light was passed through a Yokogawa CSU-X1 spinning disk head (Yokogawa, Calgary, AB, Canada) and an emission filter wheel before detection with a Hamamatsu Orca EM-CCD camera (model 09100-13, Hamamatsu Photonics, Bridgewater, NJ) operated with Metamorph imaging software (v1.0.2, Molecular Devices). The camera exposure time was set to 250 ms with a gain of 200 and laser power usually set to 30%. To visualize the ER, fixed neurons immunolabeled for KDEL were excited with light provided by a 491-nm laser line while the emitted light was passed through a 502- to 537-nm band-pass emission filter. MitoTracker Red and the PMCA immunolabeling (Alexa 594) were visualized by exciting neurons with a 568-nm laser and emission light passed through a 590- to 650-nm band-pass emission filter. Images of double-labeled cultured neurons were acquired with a Leica TCS SP2 multiphoton laser scanning confocal microscope (Heidelberg, Germany) equipped with a $\times$40 (NA = 0.75) Leica objective. Excitation light was provided by a laser line, and emitted light passed through a prism and was collected by photomultiplier tubes. For each focal plane, PMCA and KDEL immunolabeling were measured. To visualize the PMCA, neurons were excited with light provided by a 543-nm laser line, while the emitted light was collected from a bandwidth range between 575 and 615 nm. Conversely, KDEL immunolabeling was assessed by excitation with a 488-nm argon laser, while fluorescent emission was collected from a bandwidth range between 515 and 535 nm.

Confocal imaging stacks of ~30–40 horizontal optical sections of 1- to 2-μm thickness were acquired along the entire vertical axis and saved for off-line analysis in ImageJ (v1.43; http://rsbweb.nih.gov/ij/). Images used for presentation were taken from the central portion of the soma in either the horizontal (x,y axes) or vertical (x,z and y,z) planes. A horizontal section divided the soma into upper (furthest from the glass bottom) and bottom (nearest the glass substrate) sections. Conversely, a vertical section divided the soma into left and right halves when viewing the dish perpendicular to the glass coverslip. Images presented as vertical cross sections were reconstructed with ImageJ by taking fluorescence measurements in the middle of the soma along the x- or y-axis of a given horizontal optical section. The measurements from each horizontal section in the entire image stack were then compiled to form a vertical optical section of the soma. Each horizontal optical section constituted 1 pixel (1–2 μm/pixel) in the z-axis of the vertical optical section, while the pixel density in the horizontal plane (x- or y-axis) was 0.227 μm/pixel. Thus, unlike horizontal sections, pixels in the scaled vertical cross sections were rectangular, not square.

Immunohistochemistry for KDEL was also performed on sections of bag cell neuron clusters from the abdominal ganglion. Abdominal ganglia were dissected from the animal (see *Animals and Cell Culture*) and fixed overnight at room temperature in 4% paraformaldehyde with 30% sucrose in 0.1 M sodium phosphate buffer (0.1 M $NaHPO_4 \cdot H_2O$ and 0.1 M $NaHPO_4 \cdot 7H_2O$) pH 7.3 with NaOH. The next day, ganglia were rinsed four times, 10 min each, at room temperature in 30% sucrose in sodium phosphate buffer. Fixed ganglia were tamped dry, mounted in Optimal Cutting Temperature embedding medium (4583, Miles, Elkhart, IN), frozen at −80°C, and cut into 6-μm coronal sections with a cryostat microtome. Sections were mounted on Superfrost Plus slides (12-550-15, Fisher Scientific) and stored at −20°C until being used.

Tissue sections were permeabilized for 10 min at room temperature with 2% (wt/vol) Triton X-100 in PBS (composition in mM: 137 NaCl, 2.7 KCl, 4.3 Na_2HPO_4, pH 7.0 with NaOH). After being washed four times, 10 min each, with PBS, sections were blocked for 30 min at room temperature in a blocking solution of 5% (vol/vol) goat serum in PBS. Rat anti-KDEL primary was applied at 1:200 in blocking solution, and sections were incubated overnight at 4°C in the dark. Sections were then washed four times, 10 min each, with PBS and incubated for 1 h in the dark at room temperature in 1:200 secondary goat anti-rabbit IgG conjugated to Alexa Fluor 488. Sections were then washed four times, 10 min each, with PBS, mounted in mounting medium, and covered with a glass coverslip.

Stained abdominal ganglion tissue sections were imaged with a Nikon TS100-F inverted microscope equipped with Nikon Plan Fluor $\times$10 (NA = 0.3) or Nikon Plan Fluor $\times$20 oil-immersion (NA = 0.75) objectives. Neurons were excited with a 50-W Hg lamp and a 480/15-nm band-pass filter. Fluorescence was emitted to the eyepiece or camera through a 505-nm dichroic mirror and a 520-nm barrier filter. For KDEL imaging (Alexa Fluor 488), neurons were excited with light supplied by a 50-W Hg lamp that was first passed through a 480/15-nm band-pass filter. Fluorescence was emitted to the eyepiece or camera through a 505-nm dichroic mirror and a 520-nm barrier filter. Images were acquired at the focal plane of either the neurites or soma with a Pixelfly USB camera (PCO-TECH, Photon Technology International) and the

Micro-Manager (v1.4.5 http://micro-manager.org) plug-in for ImageJ with 100- to 2,000-ms exposure times.

Reagents and Drug Application

Solution exchanges were accomplished by manual perfusion using a calibrated transfer pipette to first exchange the bath (tissue culture dish) solution. In most cases where a drug was applied, a small volume (2–10 μl) of concentrated stock solution was mixed with a larger volume of saline (100–150 μl) that was initially removed from the bath, and this mixture was then pipetted back into the bath. Carbonyl cyanide *p*-trifluoromethoxyphenylhydrazone (FCCP; 21857, Sigma-Aldrich), carboxyeosin (C-22803, Invitrogen), ryanodine (559276, Calbiochem, San Diego, CA), and cyclopiazonic acid (CPA; C1530, Sigma-Aldrich or 239805, Calbiochem) all required DMSO as a vehicle. The maximal final concentration of DMSO was 0.5% (vol/vol), which in control experiments as well as prior work from our laboratory had no effect on membrane potential, various macroscopic or single-channel currents, resting intracellular Ca^{2+}, or Ca^{2+} transients evoked by a train of action potentials (Gardam et al. 2008; Geiger and Magoski 2008; Hickey et al. 2010; Hung and Magoski 2007; Kachoei et al. 2006; Lupinsky and Magoski 2006; Tam et al. 2009, 2011). Tetraphenylphosphonium chloride (TPP; 218790, Sigma-Aldrich) was prepared in water.

Analysis

Origin (v7, OriginLab, Northampton, MA) was used to import and plot ImageMaster Pro files as line graphs. Analysis of intracellular Ca^{2+} usually compared the steady-state value of the baseline 340/380 with the ratio from regions that had reached a peak or new steady state. Measurements of the baseline and peak regions were determined by eye or with five-point adjacent-averaging in Origin. CICR magnitude and the extent of Ca^{2+} removal after a stimulus train were quantified with measurements of posttrain area, but over different time periods. During circumstances where CICR was present, area was calculated by integrating the region above the prestimulus baseline from 1 to 11 min after the train. Measurements began at 1 min after the train to capture peak CICR and avoid including the initial recovery from Ca^{2+} influx. Under circumstances where CICR was eliminated with TPP, which inhibits mitochondrial Ca^{2+} exchangers (Karadjov et al. 1986; Wingrove and Gunter 1986), the efficacy of posttrain Ca^{2+} removal was quantified by measuring the area above baseline between immediately after the train to 10 min later. This timespan captures both the initial and late periods of posttrain Ca^{2+} decay. To plot the rate of Ca^{2+} removal as a function of intracellular Ca^{2+}, the slope [(340/380)/*t*] of the posttrain decay period was determined at sequential time points with Excel (v14, Microsoft, Redmond, WA). A fitted slope was measured from the initial point of posttrain Ca^{2+} decay over the next five sequential time points, while incrementally shifting the start time until the end of the decay period. From this, a plot of Ca^{2+} decay rate vs. 340/380 was produced and fit with a polynomial function in Excel. The mitochondrial rate component (R_{mit}) was discerned by subtracting the rate of decay measured in FCCP (R_{FCCP}) from the rate of decay in the absence of FCCP (R_{cntl}).

The staining distribution of MitoTracker Red and α-KDEL was quantified in ImageJ from vertical cross sections (*x*,*z* plane) at the midpoint of the soma. Mean fluorescence intensity was assessed from regions of interest (ROIs) in the left, right, upper, and bottom domains of the soma periphery. ROIs in the left and right poles consisted of polygons that outlined a portion near the apparent plasma membrane and spanned to a vertical boundary 5 μm from the leftmost or rightmost region of the cell (see Fig. 7, *C*, *F*, and *I*). For the upper and bottom poles, ROIs captured the region spanning between the apparent membrane edge and 5 μm in the intracellular direction. The upper and bottom ROIs were 50% of the maximum width of the soma and were centered at its midpoint (see Fig. 7, *C*, *F*, and *I*). For analysis, the mean fluorescence intensity of the left, right, upper, and bottom areas of the soma were normalized to the maximum fluorescence of the four regions in a given neuron.

Summary data are presented as bar graphs and error bars representing means and SE, respectively. Statistics were performed with InStat (version 3.0, GraphPad Software, San Diego, CA). The Kolmogorov-Smirnov method was used to test data sets for normality. If the data were normal, Student's paired or unpaired *t*-test (with Welch correction or Bonferroni correction as required) was used to test for differences between two means. If the data were not normally distributed, the Mann-Whitney *U*-test was used. Comparison between multiple means was performed with an ordinary one-way analysis of variance (ANOVA) followed by Tukey's multiple-comparisons post hoc test, where each *P* value was adjusted for multiple comparisons. Unless stated otherwise, all statistical comparisons were two-tailed, and means were considered significantly different if the *P* value was <0.05.

Model Development

A compartment model of intracellular Ca^{2+} dynamics was constructed to examine the interaction between voltage-gated Ca^{2+} entry, plasma membrane Ca^{2+} extrusion by the PMCA, and mitochondrial Ca^{2+} fluxes. The model was adapted from the functions and parameters that describe a similar phenomenon involving stimulus-evoked Ca^{2+} dynamics and mitochondrial Ca^{2+} release in bullfrog sympathetic neurons (Colegrove et al. 2000a, 2000b).

Plasma membrane Ca^{2+} flux.

$$J_{influx} = k_{influx}\left(\left[Ca^{2+}\right]_i - \left[Ca^{2+}\right]_e\right) \quad (1)$$

$$J_{PMCA} = V_{max,PMCA}/\left[1 + \left(EC_{50,PMCA}/\left[Ca^{2+}\right]_i\right)^{n,PMCA}\right] \quad (2)$$

$$J_{extru} = V_{max,extru}/\left[1 + \left(EC_{50,extru}/\left[Ca^{2+}\right]_i\right)^{n,extru}\right] \quad (3)$$

$$J_{pm} = J_{influx} + J_{PMCA} + J_{extru} \quad (4)$$

where J_{influx} is the rate of Ca^{2+} influx across the plasma membrane, k_{influx} refers to the Ca^{2+} permeability of the membrane, and $[Ca^{2+}]_i$ and $[Ca^{2+}]_e$ are the intracellular and extracellular Ca^{2+} concentrations, respectively. To produce Ca^{2+} influx in the model, k_{influx} was transiently increased and then reduced manually. J_{PMCA} is the rate of plasma membrane efflux by the PMCA, $V_{max,PMCA}$ is the maximal rate of efflux by the PMCA, $EC_{50,PMCA}$ is the Ca^{2+} concentration at which J_{PMCA} is half of $V_{max,PMCA}$, and *n*,PMCA is the Hill coefficient that controls the sensitivity of J_{PMCA} to changes in cytosolic Ca^{2+}. In some of our experimental conditions, the PMCA is disrupted with carboxyeosin (a PMCA inhibitor) but CICR still recovers to prestimulus levels, indicating that a residual extrusion system must be involved. Thus we included a residual extrusion system to fulfill this function in the model and termed it J_{extru}—the rate of plasma membrane Ca^{2+} extrusion by residual Ca^{2+} removal systems. $V_{max,extru}$ is the maximal rate of extrusion, $EC_{50,extru}$ is the Ca^{2+} concentration at which J_{extru} is half of $V_{max,extru}$, and *n*,extru is the Hill coefficient. J_{pm} is the net plasma membrane Ca^{2+} flux and is determined by the combined function of plasma membrane Ca^{2+} influx (J_{influx}) and efflux (J_{PMCA} and J_{extru}).

Mitochondrial Ca^{2+} dynamics.

$$J_{uptake} = k_{max,uptake}\left[Ca^{2+}\right]_i/1 + \left(EC_{50,uptake}/\left[Ca^{2+}\right]_i\right)^{n,uptake} \quad (5)$$

$$\delta\left(\left[Ca^{2+}\right]_i\right) = 1.0 - 1.0/\left[1.0 + \left(K_{inhib}/\left[Ca^{2+}\right]_i\right)^{n,inhib}\right] \quad (6)$$

$$J_{release} = -\delta\left(\left[Ca^{2+}\right]_i\right)V_{max,release}/\left(1 + EC_{50,release}/\left[Ca^{2+}\right]_m\right) \quad (7)$$

$$J_{mito} = J_{uptake} + J_{release} \quad (8)$$

where J_{uptake} is the rate of mitochondrial Ca^{2+} sequestration, $k_{max,uptake}$ is the mitochondrial uptake rate constant and represents the limiting slope at high cytosolic Ca^{2+}, $EC_{50,uptake}$ describes the Ca^{2+} concentration at

which uptake is half-maximal, and *n*,uptake is the Hill coefficient. The factor $\delta([Ca^{2+}]_i)$ describes the inhibition of mitochondrial Ca^{2+} extrusion by cytosolic Ca^{2+}. K_{inhib} is the Ca^{2+} concentration at which inhibition of $J_{release}$ is half-maximal, and *n*,inhib describes the sensitivity of inhibition to cytosolic Ca^{2+}. $V_{max,release}$ is the maximal rate of Ca^{2+} release from the mitochondria, and $EC_{50,release}$ is the concentration of mitochondrial Ca^{2+} ($[Ca^{2+}]_m$) at which efflux rate is half of $V_{max,release}$. J_{mito} is the net Ca^{2+} flux of the mitochondria.

Exogenous Ca^{2+} buffers.

$$J_{EGTA} = k_{off}[CaB] - k_{on}[Ca^{2+}]_i[B] \quad (9)$$

where J_{EGTA} is the rate of free cytosolic Ca^{2+} removal by EGTA (Nowycky and Pinter 1993), k_{off} and k_{on} are the reverse and forward reaction constants, respectively, [Ca*B*] is the concentration of the Ca^{2+}-EGTA complex, $[Ca^{2+}]_i$ is the concentration of cytosolic Ca^{2+}, and [*B*] is the concentration of free EGTA. Values for k_{off} and k_{on} (Table 1) were taken from Naraghi (1997), whereas [Ca*B*] and [*B*] were calculated from the total EGTA concentration with MaxChelator (http://maxchelator.stanford.edu/CaEGTA-NIST.htm).

Collective Ca^{2+} dynamics.

$$d[Ca^{2+}]_i/dt = J_{pm} + J_{mito} + J_{EGTA} \quad (10)$$

$$d[Ca^{2+}]_m/dt = J_{mito}/\gamma \quad (11)$$

where $d[Ca^{2+}]_i/dt$ is the rate of change in cytosolic Ca^{2+}, $d[Ca^{2+}]_m/dt$ is the rate of change of mitochondrial Ca^{2+}, and γ is the ratio of effective mitochondrial and cytoplasmic volumes. The γ value was taken from estimates in bullfrog sympathetic neurons (Colegrove et al. 2000b). The components describing mitochondrial Ca^{2+} uptake ($EC_{50,uptake}$ and *n*,uptake) were made in accordance with measurements from isolated mitochondria (Colegrove et al. 2000b; Gunter and Gunter 1994; Gunter and Pfeiffer 1990). All other parameter values (see Table 1) were within an order of magnitude of those estimated from the bag cell neurons or bullfrog sympathetic neurons (Colegrove et al. 2000b; Groten et al. 2013). The only time-dependent component of the model was the transient change in plasma membrane Ca^{2+} permeability (k_{influx}) to produce Ca^{2+} influx; all other parameters were active throughout each simulation. Differential equations were solved numerically with Euler's method written in MATLAB (v7.6; MathWorks, Natick, MA) with a time step of 75 ms to produce graphical outputs of total cytosolic and mitochondrial Ca^{2+} over time.

RESULTS

Inhibiting Ca^{2+} Extrusion by Plasma Membrane Ca^{2+}-ATPase Unveils Large Ca^{2+} Plateau After Fast-Phase-Like Stimulus

In many neurons, the presence of CICR is highly dependent on the magnitude of Ca^{2+} influx (Colegrove et al. 2000a; Llano et al. 1994; Richter et al. 2005; Shmigol et al. 1995; Usachev and Thayer 1997). Likewise, sharp-electrode recordings from bag cell neurons have shown that CICR is only elicited by prolonged action potential firing (Geiger and Magoski 2008). Moreover, when whole cell recordings of bag cell neurons are performed with an intracellular solution containing the exogenous Ca^{2+} chelator EGTA, prolonged stimulation is insufficient to elicit CICR (Groten et al. 2013). To demonstrate this here, intracellular Ca^{2+} dynamics were measured in fura-PE3-loaded cultured bag cell neurons under whole cell voltage clamp (Fig. 1*A*, *inset*). Voltage-gated Ca^{2+} influx was initiated by delivering a 5-Hz, 1-min train of 75-ms depolarizing pulses from −80 to 0 mV, which mimics the fast phase of the afterdischarge (Kaczmarek et al. 1982; Kupfermann and Kandel 1970). Except for one set of experiments (see below), all neurons were recorded with a Cs^+-based intracellular solution and a Ca-Cs-TEA external solution to isolate Ca^{2+} currents. Cs^+ and TEA^+ were substituted for K^+ and Na^+, respectively (see *Whole Cell Voltage-Clamp Recording* for details). Although these conditions prevent the activity of the Na^+/Ca^{2+} exchanger (Blaustein and Lederer 1999; Knox et al. 1996), our prior work has shown that this has no impact on voltage-gated Ca^{2+} influx or its subsequent removal (Groten et al. 2013). In neurons treated with DMSO (the vehicle) and recorded with the standard EGTA-containing intracellular solution, the train caused a transient rise in intracellular Ca^{2+}, followed by an exponential return to prestimulus baseline levels within ~5 min ($n = 10$) (Fig. 1*A*, *left*).

We next examined the influence of PMCA function on posttrain Ca^{2+} dynamics by exposing bag cell neurons for ~10 min to carboxyeosin, a PMCA inhibitor (Gatto et al. 1995; Gatto and Milanick 1993; Shmigol et al. 1998). Carboxyeosin had no significant effect on the prestimulus Ca^{2+} concentration

Table 1. *Parameter values used in the compartment model of intracellular Ca^{2+}*

Definition	Model Variable	Value
Rate constant for plasma membrane Ca^{2+} influx	k_{influx}	5×10^{-6} s^{-1}
Extracellular Ca^{2+} concentration	$[Ca^{2+}]_e$	11 mM
$[Ca^{2+}]_i$ at half-maximal rate of PMCA extrusion	$EC_{50,PMCA}$	378.8 nM
Hill coefficient for PMCA extrusion	*n*,PMCA	1.8
Maximal rate of PMCA extrusion	$V_{max,PMCA}$	28 nM/s
$[Ca^{2+}]_i$ at half-maximal rate of residual extrusion	$EC_{50,extru}$	378.8 nM
Hill coefficient for residual extrusion	*n*,extru	1.8
Maximal rate of residual extrusion	$V_{max,extru}$	7 nM/s
$[Ca^{2+}]_i$ at half-maximal rate of mitochondrial uptake	$EC_{50,uptake}$	10 μM
Hill coefficient for mitochondrial Ca^{2+} uptake	*n*,uptake	2
Rate constant for mitochondrial Ca^{2+} uptake	$k_{max,uptake}$	10.3 s^{-1}
$[Ca^{2+}]_m$ at half-maximal rate of release	$EC_{50,release}$	307 nM
Maximal rate of mitochondrial Ca^{2+} release	$V_{max,release}$	24.8 nM/s
Mitochondrial-to-cytosolic effective volume ratio	γ	2
$[Ca^{2+}]_i$ at half-maximal release inhibition	K_{inhib}	500 nM
Hill coefficient for release inhibition	*n*,inhib	6
Dissociation constant of EGTA	$K_{d,EGTA}$	180 nM
Forward rate constant of EGTA	k_{on}	2.7×10^6 $M^{-1} \cdot s^{-1}$
Reverse rate constant of EGTA	k_{off}	0.5 s^{-1}

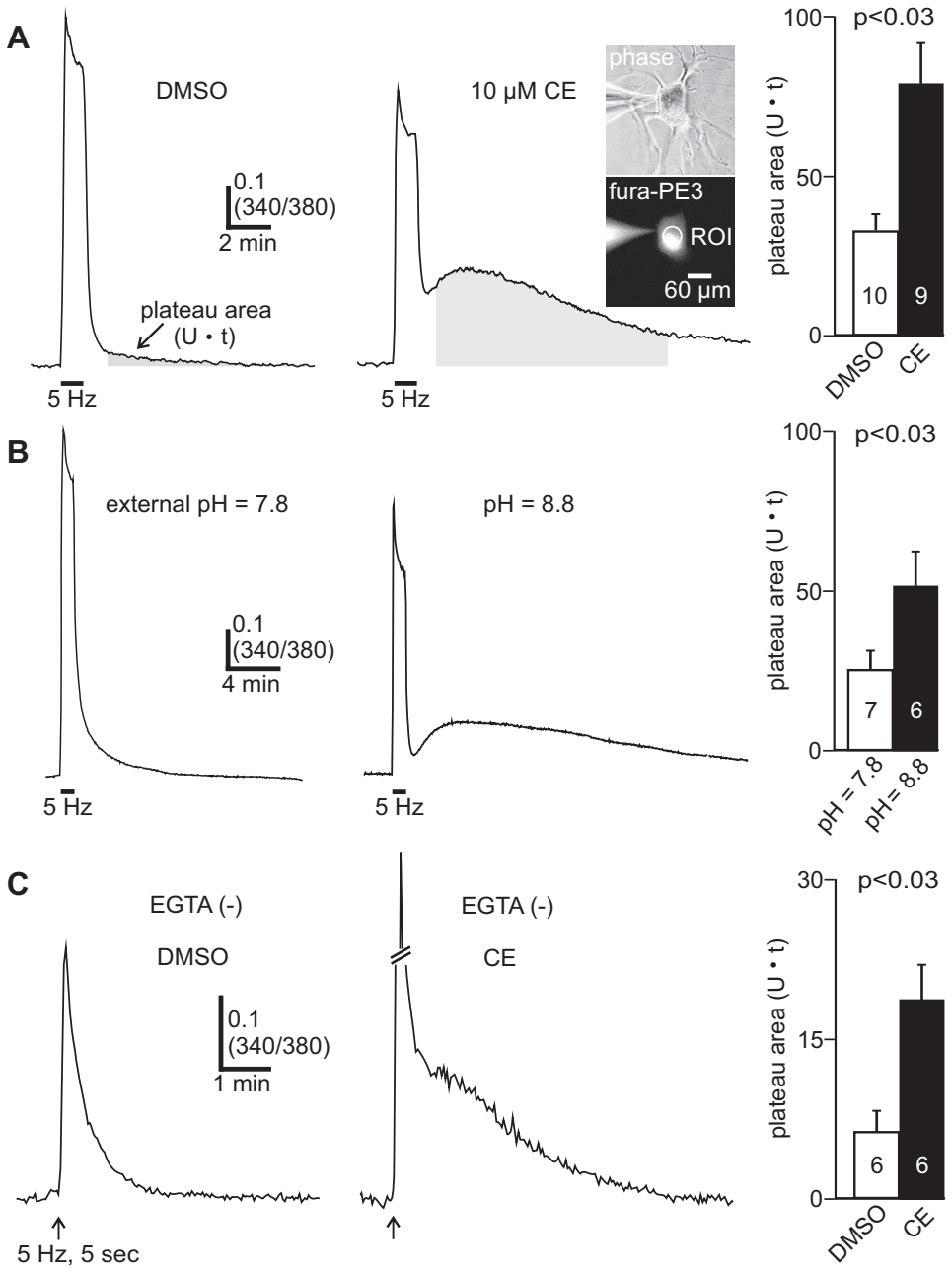

Fig. 1. Inhibiting the plasma membrane Ca^{2+}-ATPase (PMCA) unveils a large Ca^{2+} plateau following a fast-phase-like stimulus. *A*: ratiometric fluorescence measurements (340/380 nm) of intracellular Ca^{2+} from the soma of fura-PE3-loaded cultured bag cell neurons recorded under whole cell voltage clamp with our standard Cs^{+}-based intracellular solution containing the exogenous Ca^{2+} chelator EGTA. *Inset*, phase (*top*) and fura fluorescence (*bottom*) images of a bag cell neuron; the whole cell recording pipette, and the somatic region of interest (ROI) used for analysis are indicated. *Left*: a 5-Hz, 1-min train of 75-ms depolarizing steps to 0 mV from a holding potential of −80 mV activates voltage-gated Ca^{2+} channels and elicits a large rise in intracellular Ca^{2+}, as indicated by an increase in the fluorescence ratio. After the train, intracellular Ca^{2+} decays exponentially to basal levels within ~5 min because of Ca^{2+} removal systems. *Center*: in a different neuron treated for ~10 min with 10 μM carboxyeosin (CE) to disrupt the PMCA, the train elicits a transient rise in Ca^{2+}; subsequently, the Ca^{2+} partially recovers to baseline but then transitions into a prolonged elevation that long outlasts the initial stimulus duration. The posttrain Ca^{2+} signal peaks within ~2 min and returns to basal levels after 10–20 min. For analysis, we measured the plateau area [340/380 units (U)·s (*t*)] above prestimulus baseline between 1 and 11 min after the train. This timespan was used because it avoids the initial recovery period following influx and largely captures the posttrain Ca^{2+} response in most cells (see shaded gray region). *Right*: summary data showing the posttrain plateau area. Compared with control, carboxyeosin significantly augments the plateau area (unpaired Mann-Whitney U-test). For this and all subsequent bar graphs, data are means ± SE, with the number of neurons (*n*) indicated within or just above the bars. *B*, *left*: in normal external pH (pH = 7.8), the 5-Hz, 1-min train produces Ca^{2+} influx and a subsequent exponential decay to baseline after stimulation. *Center*: in contrast, cells bathed in high external pH (pH = 8.8) to inhibit the PMCA display an initial Ca^{2+} influx during the train that is followed by a sustained Ca^{2+} elevation. *Right*: compared with normal external pH, high external pH significantly increases the posttrain plateau area (unpaired 1-tailed Mann-Whitney *U*-test). *C*: ratiometric Ca^{2+} measurements acquired from cells recorded with an EGTA-free (−) intracellular solution. *Left*: applying a brief, 5-Hz, 5-s train to a DMSO-exposed neuron produces a transient Ca^{2+} response that rapidly returns to baseline. *Center*: another neuron, given carboxyeosin to inhibit the PMCA, shows a pronounced Ca^{2+} plateau in response to the 5-Hz, 5-s train stimulus. *Right*: for cells in EGTA-free conditions, the posttrain plateau area is significantly increased by carboxyeosin (unpaired Student's *t*-test).

(340/380 DMSO: 0.34 ± 0.01, $n = 10$; 340/380 carboxyeosin: 0.32 ± 0.02, $n = 9$; unpaired Student's t-test, $P > 0.05$). Delivering the 5-Hz, 1-min train produced a peak Ca^{2+} rise in carboxyeosin-treated neurons that was only slightly smaller (Fig. 1*A*, *center*) and not statistically different from cells in control conditions (DMSO peak Δ340/380: 0.69 ± 0.07, $n = 10$; carboxyeosin: 0.58 ± 0.07, $n = 9$; unpaired Student's t-test, $P > 0.05$). However, with carboxyeosin, the Ca^{2+} dynamics after the stimulus were temporally more complex and long outlasted the duration of the initial stimulus. After an early posttrain recovery, intracellular Ca^{2+} progressively increased to a plateau or second peak by 1–3 min, and then slowly returned to baseline over 10–20 min ($n = 9$) (Fig. 1*A*, *center*). The kinetics and magnitude of this response are strikingly similar to CICR (Geiger and Magoski 2008; Groten et al. 2013). The Ca^{2+} plateau size and duration were quantified by measuring the area above baseline between 1 and 11 min after the train. Measurements began at 1 min after the train to capture the peak posttrain Ca^{2+} response and avoided including the initial decay period. Relative to control, carboxyeosin exposure significantly increased the plateau area above baseline (Fig. 1*A*, *right*).

We sought to confirm the influence of Ca^{2+} extrusion by the PMCA, but with a nonpharmacological method of inhibition. Ca^{2+} export by the PMCA requires the concomitant import of protons and can be disrupted by extracellular alkalization (Niggli et al. 1982; Thomas 2011). This is a standard technique to prevent Ca^{2+} removal by the PMCA and has been successfully employed in other neuronal preparations (Shutov et al. 2013; Usachev et al. 2002). Here, the impact of increasing extracellular pH (from pH 7.8 to 8.8) was examined on train-evoked Ca^{2+} signals. As with carboxyeosin, increasing extracellular pH from pH 7.8 to 8.8 had no significant effect on the prestimulus Ca^{2+} concentration (resting 340/380 normal pH: 0.28 ± 0.01, $n = 7$; high pH: 0.32 ± 0.02, $n = 6$; unpaired Mann-Whitney U-test, $P > 0.05$). Cells in normal-pH external solution showed a transient surge in Ca^{2+} during the 1-min train and then a standard recovery to baseline ($n = 7$) (Fig. 1*B*, *left*). Conversely, neurons immersed in high-pH external solution, to hinder Ca^{2+} extrusion by the PMCA, presented a robust and protracted posttrain Ca^{2+} elevation that was indistinguishable from that seen in carboxyeosin ($n = 6$) (Fig. 1*B*, *center*). The plateau area above baseline between 1 min and 11 min after the train was significantly increased in high external pH relative to normal external pH (Fig. 1*B*, *right*). Like carboxyeosin, high external pH did not significantly alter the peak train Ca^{2+} response (DMSO peak Δ340/380: 0.76 ± 0.06, $n = 7$; carboxyeosin: 0.72 ± 0.04, $n = 6$; unpaired Student's t-test, $P > 0.05$).

Considering that our standard recording conditions contain EGTA, which influences Ca^{2+} dynamics, we examined whether protracted posttrain Ca^{2+} elevation could also be observed in the absence of this exogenous Ca^{2+} chelator. With an EGTA-free intracellular solution, cells were stimulated with a 5-Hz, 5-s train of depolarizing steps, which is a stimulus that should be subthreshold for eliciting CICR under these conditions (Geiger and Magoski 2008). In response to the 5-s train, there was a transient increase in Ca^{2+}, followed by a rapid recovery to baseline ($n = 6$) (Fig. 1*C*, *left*). In contrast, cells exposed to 10 μM carboxyeosin presented a pronounced posttrain Ca^{2+} plateau that required more time to recover to prestimulus baseline ($n = 6$) (Fig. 1*C*, *center*). This is reflected in the summary data, showing that carboxyeosin significantly increased the plateau area above baseline between 1 min and 11 min after the train (Fig. 1*C*, *right*). This response is qualitatively similar to the 1-min train-evoked Ca^{2+} dynamics seen in carboxyeosin-treated neurons recorded with EGTA-containing intracellular saline. In the EGTA-free recording conditions, neurons given carboxyeosin showed slightly greater resting Ca^{2+} levels and peak train Ca^{2+} responses relative to untreated controls. However, these differences did not reach statistical significance [resting 340/380 DMSO: 0.38 ± 0.023 ($n = 6$), carboxyeosin: 0.45 ± 0.06 ($n = 6$), unpaired Student's t-test, $P > 0.05$; DMSO peak Δ340/380: 0.31 ± 0.03 ($n = 6$), carboxyeosin: 0.54 ± 0.11 ($n = 6$), unpaired Welch corrected Student's t-test, $P > 0.05$].

The Posttrain Ca^{2+} Plateau That Occurs in Absence of PMCA Activity Is Mediated by Ca^{2+} Release from Mitochondria but Not ER

The delayed Ca^{2+} peak and prolonged Ca^{2+} elevation that is unveiled in the absence of PMCA activity may represent intracellular Ca^{2+} release (Geiger and Magoski 2008; Groten et al. 2013). However, the prolonged Ca^{2+} elevation could be mediated by other processes, such as reduced removal of cytosolic Ca^{2+}. Thus we examined the contribution of intracellular Ca^{2+} release to the 1-min train-evoked Ca^{2+} plateau seen in carboxyeosin. All subsequent recordings were performed with our standard EGTA-containing Cs^{+}-based intracellular solution. In many other types of neurons, CICR occurs when voltage-gated Ca^{2+} influx triggers Ca^{2+} release through ryanodine receptors on the ER membrane (Verkhratsky 2005). To test whether this was the case for bag cell neurons, 100 μM ryanodine, a dose that inhibits ryanodine receptor-derived Ca^{2+} release (Meissner 1985; Verkhratsky 2005), was used. Compared with 10 μM carboxyeosin alone ($n = 6$), a 10-min treatment with 100 μM ryanodine in carboxyeosin ($n = 7$) had no obvious effect on the Ca^{2+} plateau area after the 1-min train, with no significant difference between the group data (Fig. 2, *A* and *B*).

Given the negative ryanodine result, we next investigated a role for mitochondrial Ca^{2+} release. Mitochondrial CICR can be prevented by inhibiting mitochondrial Ca^{2+} exchangers with TPP (Geiger and Magoski 2008; Groten et al. 2013; Lee et al. 2013). As a control, we first discerned the impact of TPP on Ca^{2+} influx and removal in the absence of carboxyeosin, when PMCA activity is not altered. As there is no apparent Ca^{2+} release under these conditions, TPP would not be expected to influence Ca^{2+} dynamics. Relative to H_2O (the vehicle), TPP did not significantly impact resting Ca^{2+} levels (resting 340/380 H_2O: 0.26 ± 0.01, $n = 8$; TPP: 0.26 ± 0.02, $n = 6$; unpaired Student's t-test, $P > 0.05$) or peak train Ca^{2+} influx (peak Δ340/380 H_2O: 1.03 ± 0.076, $n = 8$; Δ340/380 TPP: 0.878 ± 0.11, $n = 6$; unpaired Student's t-test, $P > 0.05$). Moreover, in response to the 5-Hz, 1-min train, TPP-treated neurons ($n = 6$) did not present a significantly different posttrain plateau area vs. controls ($n = 8$) (Fig. 2, *C* and *D*).

Subsequently, the effect of TPP on train-evoked Ca^{2+} dynamics was examined when the PMCA was blocked. Again, in 10 μM carboxyeosin, the train resulted in a delayed Ca^{2+} plateau after the Ca^{2+} influx signal ($n = 12$) (Fig. 2*E*, *left*).

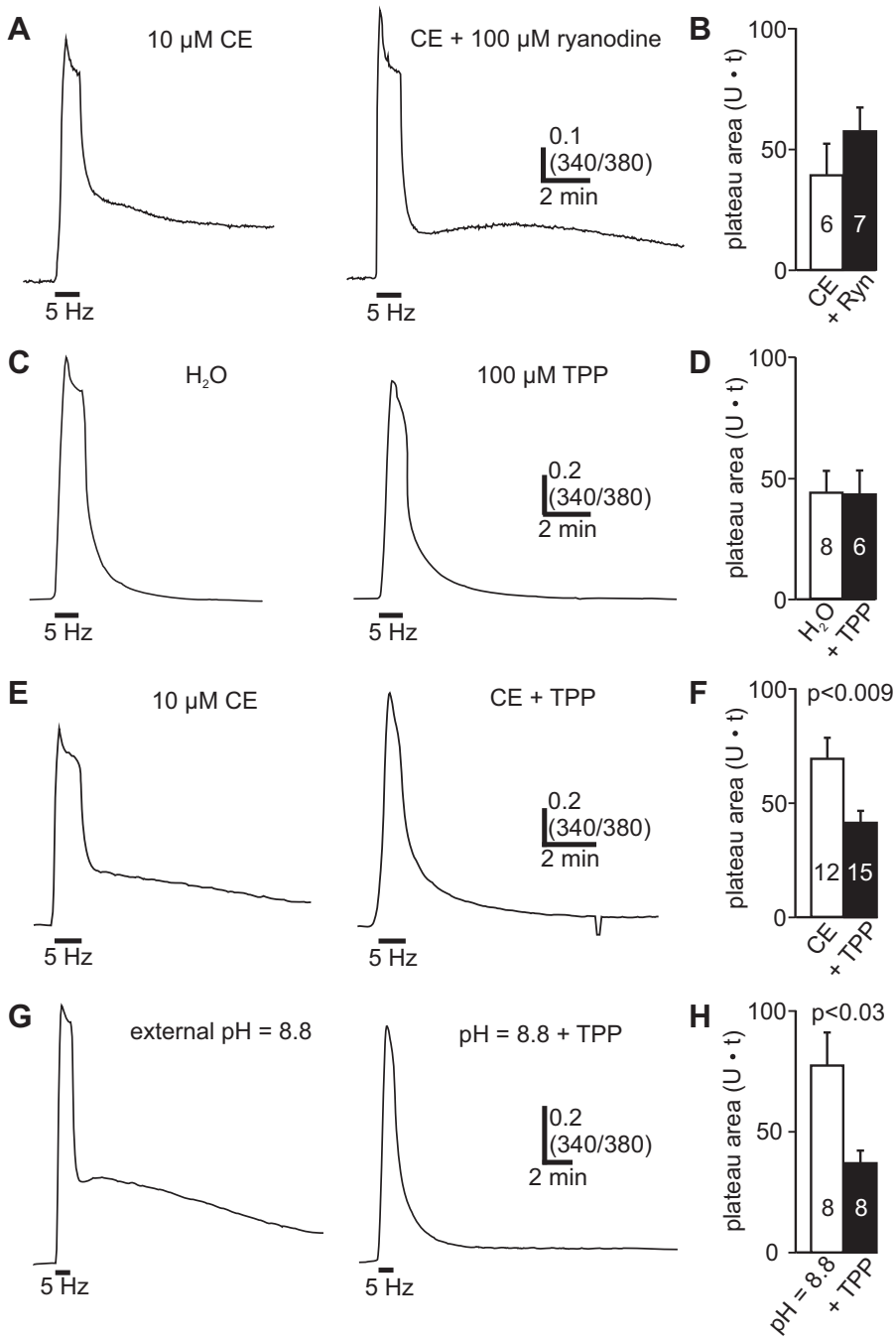

Fig. 2. The carboxyeosin-dependent posttrain Ca^{2+} plateau is mediated by Ca^{2+} release from the mitochondria. *A*, *left*: in the presence of carboxyeosin (CE), the 5-Hz, 1-min train produces a prolonged poststimulus Ca^{2+} plateau. This and all subsequent recordings were performed with our standard EGTA-containing intracellular solution. *Right*: pretreating neurons with high-concentration (100 μM) ryanodine does not appreciably alter the posttrain Ca^{2+} dynamics in a neuron exposed to 10 μM carboxyeosin. *B*: ryanodine does not significantly alter the posttrain plateau area (1–11 min after train) seen in the presence of carboxyeosin (unpaired Student's *t*-test). *C*, *left*: in control conditions (H_2O), a neuron shows a rapid exponential recovery to baseline after the 5-Hz, 1-min train. *Right*: another neuron, exposed to 100 μM TPP for 30 min to inhibit mitochondrial Ca^{2+} exchangers, presents a peak-train Ca^{2+} response and posttrain Ca^{2+} decay that is indistinguishable from control. *D*: with the PMCA active, TPP does not significantly alter the posttrain Ca^{2+} plateau area relative to control (unpaired Student's *t*-test). *E*, *left*: in the presence of carboxyeosin, the train evokes a large posttrain Ca^{2+} elevation. *Right*: in TPP + carboxyeosin, there is a similar train-evoked Ca^{2+} influx, but subsequently Ca^{2+} returns quickly to prestimulus baseline without an ensuing Ca^{2+} elevation. The transient decrease in the 340-to-380 ratio in the latter portion of the recording is an artifact caused by a brief, incidental closure of the light shutter. *F*: in the presence of carboxyeosin, the Ca^{2+} plateau area is significantly reduced by TPP (unpaired Student's *t*-test). *G*: disrupting the PMCA with high external pH (pH = 8.8) results in a posttrain Ca^{2+} elevation that is eliminated by TPP. *H*: in high-pH external, TPP significantly reduces the plateau area compared with high pH alone (Welch corrected unpaired Student's *t*-test).

Conversely, delivering a train to neurons given both carboxyeosin and 100 μM TPP resulted in a Ca^{2+} response that decayed exponentially to baseline after the train ($n = 15$) (Fig. 2*E*, *right*). The posttrain Ca^{2+} elevation in carboxyeosin was reduced under these conditions, as indicated by the significantly smaller plateau area in TPP-treated neurons (Fig. 2*F*). We also examined the influence of TPP on the posttrain Ca^{2+} plateau produced when PMCA activity was prevented with extracellular alkalization. As before, in high-pH external solution, the train elicited a robust posttrain Ca^{2+} plateau ($n = 8$) (Fig. 2*G*, *left*). In contrast, cells bathed in high-pH external solution with TPP showed no posttrain Ca^{2+} elevation ($n = 8$) (Fig. 2*G*, *right*). This was confirmed by the summary data, showing that TPP significantly reduced the Ca^{2+} plateau in high external pH (Fig. 2*H*).

Model of Intracellular Ca^{2+} Dynamics Recapitulates Effect of PMCA Disruption on Posttrain Ca^{2+} Dynamics

Our results suggested that Ca^{2+} extrusion by the PMCA influenced the ability of stimulation to elicit CICR from the mitochondria. The precise mechanism of Ca^{2+} interplay between the PMCA and the mitochondria is unclear. In bag cell neurons, intracellular Ca^{2+} is governed by the concerted action of multiple Ca^{2+} sources and Ca^{2+} extrusion/buffering systems (Groten et al. 2013; Kachoei et al. 2006; Knox et al. 1996). Therefore, we employed a simple rate model of Ca^{2+}

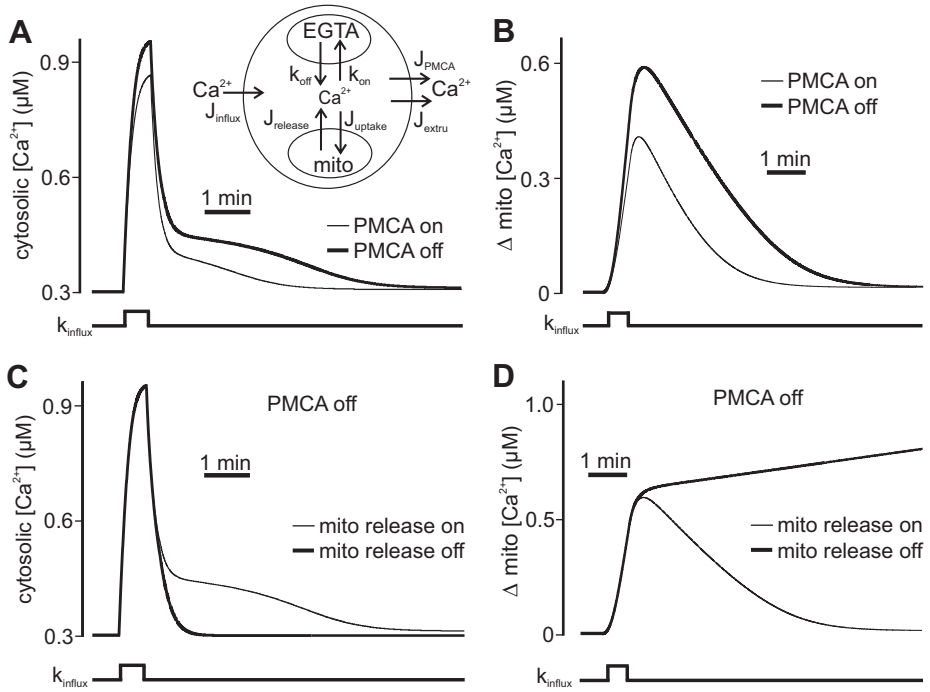

Fig. 3. A compartment model of Ca^{2+} dynamics recapitulates the influence of PMCA activity on CICR. *A*: the 3-component model of intracellular Ca^{2+} dynamics consists of extracellular, cytosolic, and mitochondrial compartments (*inset*). J_{influx} corresponds to plasma membrane Ca^{2+} influx, while J_{PMCA} and J_{extru} represent the PMCA and residual plasma membrane Ca^{2+} extrusion systems, respectively. J_{uptake} denotes mitochondrial Ca^{2+} uptake, and $J_{release}$ signifies Ca^{2+} release into the cytosol by the mitochondrial Ca^{2+} exchangers. Cytosolic Ca^{2+} buffering by the exogenous Ca^{2+} chelator EGTA is determined by its forward (k_{on}) and reverse (k_{off}) rate constants. All model presentations were derived with functions and parameter values (Table 1) consistent with the relevant literature on this topic (see *Model Development* for details). Train-induced voltage-gated Ca^{2+} influx is produced in the model by increasing the plasma membrane Ca^{2+} influx rate constant (k_{influx}). With J_{PMCA} functional (light trace), a transient change in k_{influx} elicits a rise in cytosolic Ca^{2+} and an ensuing response that contains a small Ca^{2+} shoulder. In another simulation, where J_{PMCA} was eliminated (dark trace), triggering the same k_{influx} produces a slightly larger cytosolic Ca^{2+} rise and a prominent Ca^{2+} plateau, similar to that seen physiologically during carboxyeosin treatment. *B*: changes in mitochondrial Ca^{2+} concentration occurring in response to cytosolic Ca^{2+} influx in the presence and absence of J_{PMCA}. Compared with simulations when all components are functional (light trace), eliminating J_{PMCA} (dark trace) leads to a greater increase in mitochondrial Ca^{2+} loading by Ca^{2+} influx. *C*: cytosolic Ca^{2+} influx and release when the PMCA (J_{PMCA}) is not functional and the rate of mitochondrial Ca^{2+} release ($J_{release}$) is varied to mimic the effect of TPP. Relative to when it is active (light trace), eliminating $J_{release}$ (dark trace) prevents the Ca^{2+} plateau seen when J_{PMCA} is off. *D*: corresponding changes in mitochondrial Ca^{2+} in the absence of J_{PMCA} function but with altered mitochondrial Ca^{2+} release ($J_{release}$). The decay of mitochondrial Ca^{2+} that occurs when the $J_{release}$ is functional (light trace) is prevented after the latter is inactive (dark trace).

dynamics, consisting of these primary components, in an attempt to recapitulate our findings and provide information on underlying mechanisms. Such models have proven helpful for explaining stimulus-evoked changes in cytosolic Ca^{2+} and CICR in the other systems (Colegrove et al. 2000b; Friel and Tsien 1994; Gabso et al. 1997).

The model consisted of extracellular, intracellular, and mitochondrial compartments (Fig. 3*A*, *inset*) (see *Model Development* for details). Ca^{2+} influx across the plasma membrane was mediated by J_{influx}, while plasma membrane Ca^{2+} efflux was controlled by J_{PMCA} and J_{extru}, reflecting the function of the PMCA and residual Ca^{2+} extrusion systems, respectively. The movement of Ca^{2+} into and out of the mitochondrial compartment are represented by J_{uptake} and $J_{release}$, respectively. As the ER does not contribute to Ca^{2+} removal following voltage-gated Ca^{2+} influx (Geiger and Magoski 2008; Groten et al. 2013), it was not included in the model. Finally, Ca^{2+} buffering by the exogenous Ca^{2+} chelator EGTA was contributed by J_{EGTA}.

Figure 3, *A* and *B*, show simulated changes in cytosolic and mitochondrial Ca^{2+} resulting from a transient increase in the plasma membrane Ca^{2+} permeability coefficient (k_{influx}). This is meant to reflect the opening of voltage-gated Ca^{2+} channels during a train stimulus. When all components of the model were active, turning on k_{influx} produced a rise in cytosolic Ca^{2+}, followed by a rapid Ca^{2+} removal (Fig. 3*A*). In parallel, the cytosolic Ca^{2+} elevation due to influx caused mitochondrial Ca^{2+} concentration to grow, after which it returned to basal levels because of the function of the Ca^{2+} release parameter ($J_{release}$) (Fig. 3*B*). The extruded mitochondrial Ca^{2+} produced only a slight cytosolic Ca^{2+} response when J_{PMCA} was functional. The impact of blocking the PMCA with carboxyeosin or extracellular alkalization was modeled by repeating the same simulations but with J_{PMCA} eliminated. Under these conditions, transiently activating k_{influx} resulted in a large cytosolic Ca^{2+} influx, followed by a more substantial poststimulus Ca^{2+} elevation (Fig. 3*A*). Simulated mitochondrial Ca^{2+} concentration showed that eliminating PMCA function produced greater Ca^{2+} loading of the store by Ca^{2+} influx (Fig. 3*B*). The contribution of mitochondrial Ca^{2+} release to cytosolic Ca^{2+} was demonstrated by repeating the simulation with $J_{release}$ off. Eliminating mitochondrial Ca^{2+} release (Fig. 3*D*) had no influence on the initial increase in mitochondrial Ca^{2+} but prevented its subsequent reduction vs. intact Ca^{2+} release (Fig. 3*D*). Furthermore, the posttrain Ca^{2+} plateau,

normally seen in the absence of J_{PMCA}, was eliminated without Ca^{2+} release from the mitochondria (Fig. 3*C*).

Inhibiting Ca^{2+} Extrusion by PMCA Enhances Involvement of Mitochondrial Ca^{2+} Uptake in Response to Voltage-Gated Ca^{2+} Influx

The compartment model of intracellular Ca^{2+} dynamics suggested that disrupting plasma membrane Ca^{2+} extrusion by the PMCA could facilitate CICR by making Ca^{2+} more available for mitochondrial Ca^{2+} uptake during stimulation. Thus we examined whether the relative contribution of the mitochondria to the removal of Ca^{2+} derived from voltage-gated Ca^{2+} channels is augmented when Ca^{2+} extrusion by the PMCA is prevented. If this occurs, then carboxyeosin should increase the sensitivity of posttrain Ca^{2+} decay to the disruption of mitochondrial Ca^{2+} sequestration with FCCP. This protonophore reduces the mitochondrial proton motive force and thereby collapses the inner mitochondrial membrane potential that is required for Ca^{2+} uptake into the matrix (Babcock et al. 1997; Heytler and Prichard 1962). In the following experiments, posttrain Ca^{2+} removal was studied in isolation from CICR by treating neurons with 100 μM TPP. A low FCCP concentration (200 nM) was used, to avoid the enhanced rundown of voltage-gated Ca^{2+} current that occurs with higher amounts (μM range) (Groten et al. 2013). In addition, our earlier work showed that mitochondrial Ca^{2+} liberated by FCCP can depolarize bag cell neurons by opening a nonselective cation channel (Hickey et al. 2010). However, all of the present Ca^{2+} measurements were carried out under voltage clamp at -80 mV, meaning that FCCP could not have depolarized the membrane potential or caused erroneous voltage-gated Ca^{2+} influx.

DMSO-treated neurons were first given the 5-Hz, 1-min train as a control. After full recovery of Ca^{2+} to baseline, cells were exposed to 200 nM FCCP for ~10 min and then received a second 1-min train ($n = 11$). As displayed in Fig. 4*A*, *left*, posttrain Ca^{2+} removal occurred more slowly after FCCP treatment. These results are consistent with our prior work that showed a similar, albeit larger, effect of FCCP on posttrain Ca^{2+} decay at higher concentrations (20 μM) (Geiger and

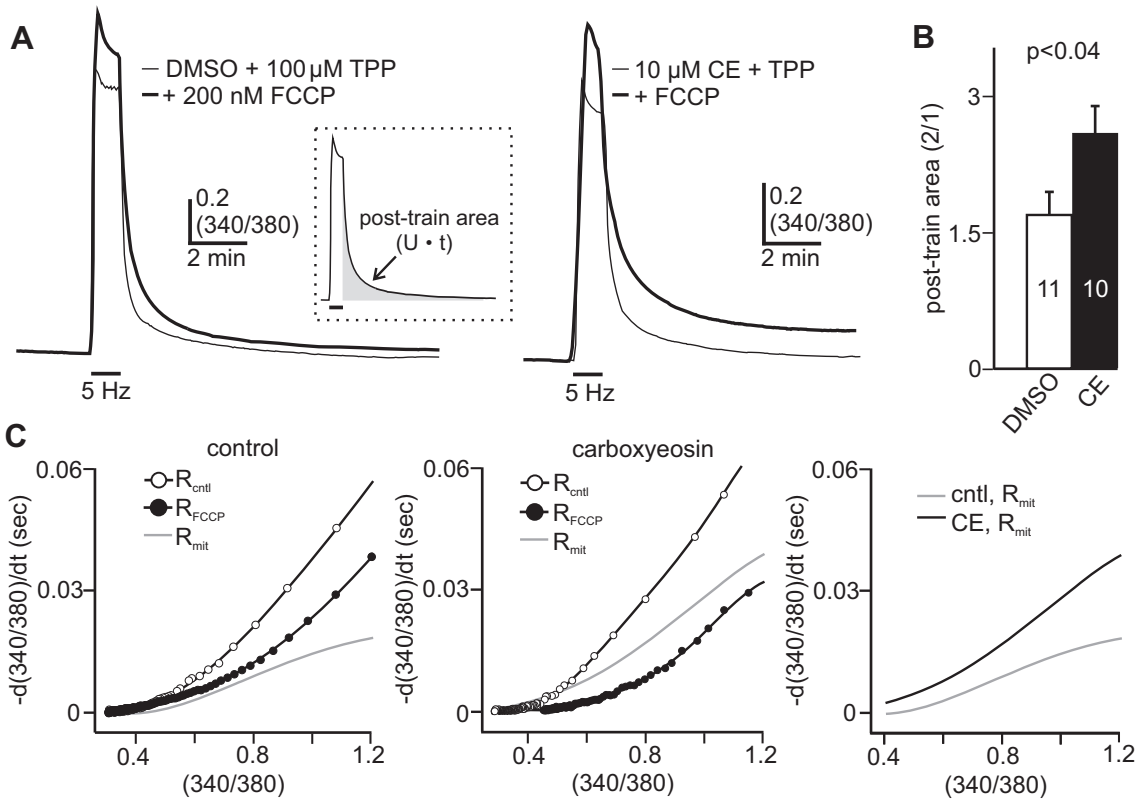

Fig. 4. Disrupting the PMCA enhances mitochondrial involvement in the removal of Ca^{2+} from voltage-gated influx after a train. *A*, *left*: applying the 5-Hz, 1-min train to a DMSO-exposed cell elicits an increase in cytosolic Ca^{2+} followed by an exponential return to baseline (light trace). After disruption of mitochondrial Ca^{2+} uptake with 200 nM FCCP for ~10 min, a second train produces a similarly sized Ca^{2+} influx signal as in the absence of FCCP, but the posttrain Ca^{2+} recovery is slowed (dark trace). All experiments are performed in 100 μM TPP to isolate the Ca^{2+} removal process from any potential CICR. *Inset*: the efficacy of posttrain Ca^{2+} removal was determined by measuring the area [340/380 units (U)·s (*t*)] above baseline between the end of the train and 10 min later (10 min total) (shaded region). *Right*: in another cell, continuously bathed in 10 μM carboxyeosin (CE), a train produces Ca^{2+} influx and a subsequent recovery (light trace). After the addition of 200 nM FCCP (still in carboxyeosin), a second train evokes Ca^{2+} influx that recovers to baseline more slowly (dark trace). Note that the effect of FCCP on posttrain Ca^{2+} removal is more substantial in the presence of carboxyeosin (*right*) than in DMSO (*left*). *B*: the ratio (*2*/*1*) of posttrain area between the second train (*2*) in FCCP and the first train (*1*) in DMSO is significantly enhanced by carboxyeosin (unpaired Student's *t*-test). *C*: Ca^{2+} clearance rate (R), acquired from the decay period of Ca^{2+} transients shown in *A*, as a function of 340-to-380 ratio. Fitted polynomial functions are plotted over the data points. The difference between control (R_{cntl}) and FCCP (R_{FCCP}) is used to produce the estimated mitochondrial uptake rate (R_{mit}) (see *Analysis* for details). *Left*: in the absence of carboxyeosin (control), the rate of Ca^{2+} clearance [d(340/380)/d*t*] has a moderate R_{mit} component over the range of Ca^{2+} measured. *Center*: in carboxyeosin, R_{mit} constitutes a large fraction of the total Ca^{2+} clearance rate over the entire Ca^{2+} range. *Right*: in carboxyeosin, R_{mit} is larger than DMSO control (cntl) and increases more steeply with changes in intracellular Ca^{2+} (340/380). R_{mit} curves are replotted from *left* and *center*.

Magoski 2008; Groten et al. 2013). Next, we repeated the experiment but with cells bathed in 10 μM carboxyeosin, to disrupt Ca^{2+} removal by the PMCA. The first train produced robust Ca^{2+} influx and an exponential recovery to baseline (Fig. 4*A*, *right*). Delivering the second train, after FCCP delivery, produced prominent Ca^{2+} influx, but the Ca^{2+} removal was substantially slowed ($n = 10$) (Fig. 4*A*, *right*). We compared the involvement of the mitochondria in posttrain Ca^{2+} removal between DMSO- and carboxyeosin-treated neurons by measuring the extent to which FCCP enhanced the posttrain area in each condition. The time frame used for this analysis spanned from the end of the train to 10 min after the train and was well-suited to capturing the initial and later periods of posttrain Ca^{2+} recovery (Fig. 4*A*, *inset*). The ratio of posttrain area between before and after FCCP was significantly larger in cells exposed to carboxyeosin (Fig. 4*B*).

Using the decay of the train Ca^{2+} responses, we also evaluated the influence of carboxyeosin on the apparent rate of mitochondrial Ca^{2+} uptake (R_{mit}) as a function of intracellular Ca^{2+} (see *Analysis* for details). R_{mit} (i.e., the FCCP-sensitive rate component) was derived by subtracting the residual removal rate in FCCP (R_{FCCP}) from the removal rate in control conditions (R_{cntl}). Figure 4*C* displays the relationship between these rate components and intracellular Ca^{2+} in the absence (Fig. 4*C*, *left*) and presence (Fig. 4*C*, *center*) of carboxyeosin. In DMSO, mitochondrial Ca^{2+} uptake occurred throughout the range of Ca^{2+} measured and increased moderately with intracellular Ca^{2+} (Fig. 4*C*, *left*). In carboxyeosin, the mitochondrial Ca^{2+} uptake rate was larger and increased more steeply to changes in intracellular Ca^{2+} (Fig. 4*C*, *center* and *right*).

Hindering Ca^{2+} Extrusion by PMCA Enhances Amount of Ca^{2+} Stored in Mitochondria After Train Stimulus

Our results suggested that preventing Ca^{2+} handling by the PMCA enhanced the contribution of the mitochondria to the removal of Ca^{2+} derived from voltage-gated Ca^{2+} channels. Consequently, carboxyeosin should increase the level of Ca^{2+} in the mitochondria after stimulation. In addition to preventing Ca^{2+} uptake, FCCP causes the liberation of stored mitochondrial Ca^{2+} (Friel and Tsien 1994; Geiger and Magoski 2008; Groten et al. 2013; Zenisek and Matthews 2000). Therefore, we assessed the amount of mitochondrial Ca^{2+} loading by treating bag cell neurons with FCCP, subsequent to the 5-Hz, 1-min train. All neurons were given 100 μM TPP to ensure that mitochondrial Ca^{2+} was not released via Ca^{2+} exchangers

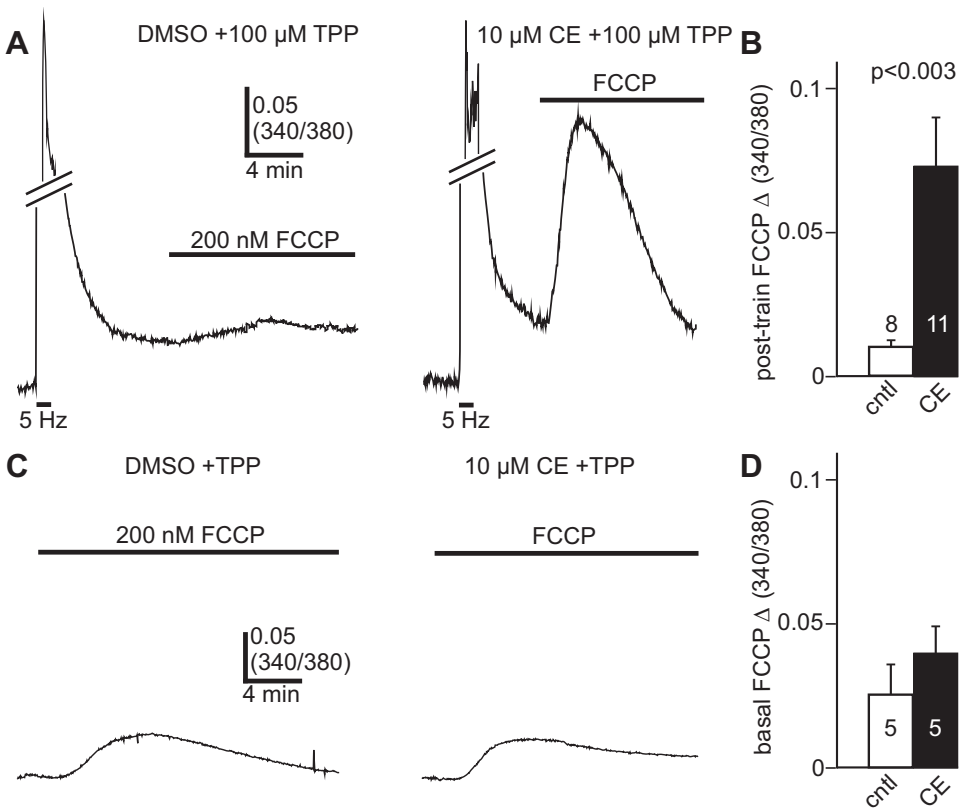

Fig. 5. Blocking the PMCA increases the loading of the mitochondrial Ca^{2+} store by voltage-gated Ca^{2+} influx. *A*, *left*: after recovery from the 5-Hz, 1-min train in DMSO, application of 200 nM FCCP produces a small Ca^{2+} response due to the liberation of stored mitochondrial Ca^{2+}. *Right*: in 10 μM carboxyeosin (CE), delivering FCCP after a train elicits a comparatively larger Ca^{2+} signal. TPP (100 μM) is present in both conditions to ensure that the mitochondrial Ca^{2+} load was not reduced by posttrain Ca^{2+} release. Line breaks in both traces omit a portion of the Ca^{2+} influx signal during the train to emphasize the Ca^{2+} liberation by FCCP. *B*: compared with DMSO controls, the peak change in FCCP-induced Ca^{2+} release following the train is significantly larger in cells given carboxyeosin (Welch corrected unpaired Student's *t*-test with Bonferroni's correction for multiple comparisons; threshold for significance $P < 0.025$). *C*, *left*: delivering 200 nM FCCP to a DMSO-exposed neuron, without a prior train stimulus, produces a relatively small Ca^{2+} increase. *Right*: in another cell exposed to carboxyeosin, FCCP elicits a Ca^{2+} signal that is not substantially different in magnitude from control. As per *A* and *B*, TPP is included in both experimental conditions. *D*: the peak change in Ca^{2+} to FCCP is not significantly different between DMSO and carboxyeosin when a prior train stimulus is not given (unpaired Student's *t*-test with Bonferroni's correction for multiple comparisons; threshold for significance $P < 0.025$).

after stimulation. In cells exposed only to DMSO, delivering 200 nM FCCP after the train produced a small, slow-rising Ca^{2+} signal ($n = 8$) (Fig. 5*A*, *left*). Conversely, in neurons that were continuously bathed in 10 μM carboxyeosin, applying 200 nM FCCP after the train resulted in markedly greater Ca^{2+} liberation ($n = 11$) (Fig. 5*A*, *right*). Indeed, compared with DMSO control, the peak FCCP-induced Ca^{2+} response was significantly augmented by carboxyeosin (Fig. 5*B*).

Carboxyeosin appears to facilitate the extent of mitochondrial Ca^{2+} loading by voltage-gated Ca^{2+} influx. However, it is possible that it alters the FCCP-dependent Ca^{2+} signal by other means. For example, disrupting Ca^{2+} removal by the PMCA could directly escalate the Ca^{2+} response by preventing its extrusion from the cytosol. Alternatively, carboxyeosin might augment mitochondrial Ca^{2+} loading under basal conditions, without voltage-gated Ca^{2+} influx. Thus, as a control, FCCP-evoked Ca^{2+} release was measured in the presence and absence of carboxyeosin, without prior train stimulation. Cells were also given 100 μM TPP to maintain consistency with prior experiments. In carboxyeosin ($n = 5$), the Ca^{2+} release signal to FCCP was not significantly different from control ($n = 5$) (Fig. 5, *C* and *D*).

Disrupting Ca^{2+} Removal by PMCA Does Not Change Contribution of ER to Removal of Ca^{2+} from Voltage-Gated Influx

Ca^{2+} handling by the PMCA appears to influence the amount of Ca^{2+} available for mitochondrial Ca^{2+} uptake in response to voltage-gated Ca^{2+} influx. Whether an analogous Ca^{2+} interplay occurs between the PMCA and other intracellular Ca^{2+} stores, such as the ER, is unclear. Ca^{2+} sequestration by the ER occurs through the sarcoplasmic/endoplasmic reticulum Ca^{2+}-ATPase (SERCA) (Berridge 2002) and in the bag cell neurons has a lesser role in the handling of Ca^{2+} derived from voltage-gated Ca^{2+} influx (Geiger and Magoski 2008; Groten et al. 2013). We tested whether inhibiting PMCA Ca^{2+} extrusion with carboxyeosin could enhance the sensitivity of posttrain Ca^{2+} removal to CPA—an inhibitor of SERCA activity (Seidler et al. 1989). For these experiments, neurons were bathed in 100 μM TPP to prevent CICR from the mitochondria and isolate posttrain Ca^{2+} removal. As seen previously, in the presence of 10 μM carboxyeosin the 5-Hz, 1-min train elicited voltage-gated Ca^{2+} influx and a subsequent recovery to baseline ($n = 7$) (Fig. 6*A*). In other neurons, given both carboxyeosin and 20 μM CPA ($n = 7$), prestimulus Ca^{2+} levels were significantly increased relative to carboxyeosin alone (resting 340/380, carboxyeosin: 0.26 $\pm$ 0.01, $n = 7$; carboxyeosin + CPA: 0.36 $\pm$ 0.03, $n = 7$; Welch corrected unpaired Student's *t*-test, $P < 0.02$). The higher basal Ca^{2+} under these conditions is likely due to the release of stored ER Ca^{2+} by CPA (Groten et al. 2013; Kachoei et al. 2006). Despite this, the train elicited Ca^{2+} influx and a subsequent Ca^{2+} recovery was indistinguishable from that seen in the absence of CPA (Fig. 6*A*). This was reflected in the summary data, showing that the posttrain area was not significantly different between carboxyeosin alone and carboxyeosin plus CPA (Fig. 6*D*, *left*). Next, the relationship between the rate of Ca^{2+} removal and intracellular Ca^{2+} was evaluated using the posttrain Ca^{2+} decay periods of the data presented in Fig. 6*A*. The rate of Ca^{2+} removal across the range of Ca^{2+} measured was not substantially different between carboxyeosin (R_{CE}) and carboxyeosin plus CPA (R_{CE+CPA}) (Fig. 6*B*). Finally,

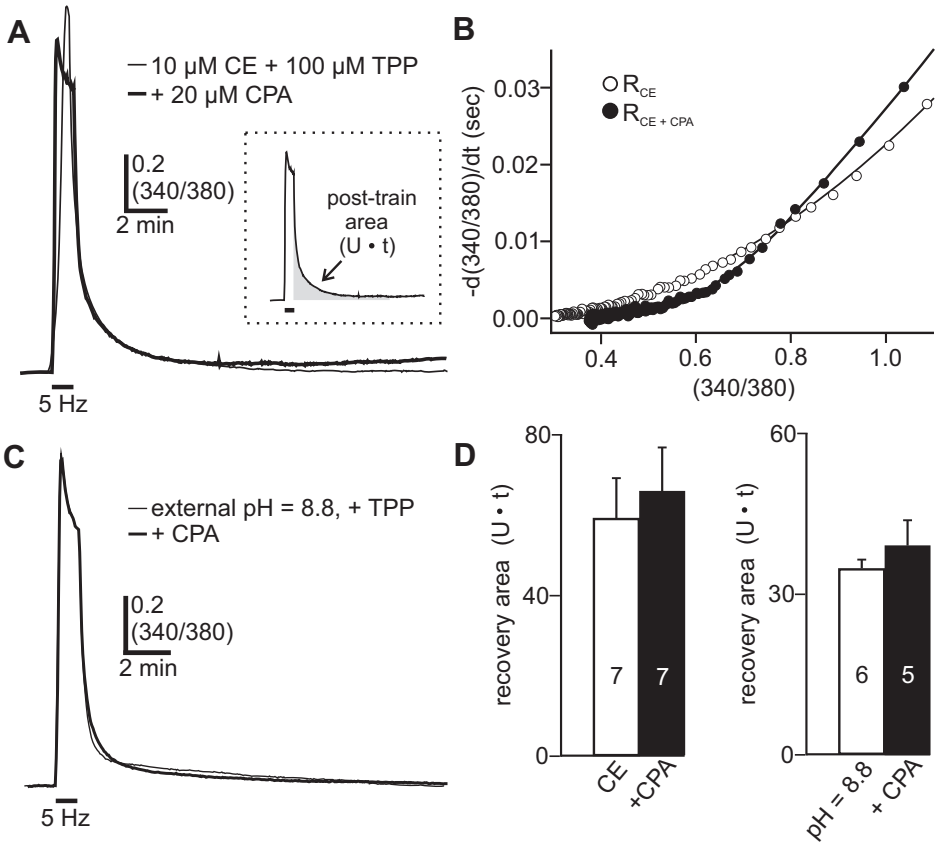

Fig. 6. PMCA disruption does not change the involvement of ER Ca^{2+} uptake during posttrain Ca^{2+} removal. *A*: compared with 10 μM carboxyeosin (CE) alone (light trace), a neuron exposed to both carboxyeosin and 20 μM CPA (to prevent Ca^{2+} uptake into the ER by the SERCA) shows very similar Ca^{2+} influx and Ca^{2+} removal in response to the 5-Hz, 1-min train. TPP (100 μM) is present in both conditions to prevent CICR and isolate the posttrain Ca^{2+} removal. *Inset*: posttrain Ca^{2+} decay was quantified by measuring the area [340/380 units (U)·s (*t*)] above baseline between the end of the train to 10 min later (shaded region). *B*: rate of Ca^{2+} removal [d(340/380)/d*t*] plotted as a function of intracellular Ca^{2+} (340/380) for the Ca^{2+} responses in *A* and fitted with polynomial functions. The total Ca^{2+} removal rate in carboxyeosin (R_{CE}) is not substantially different from the Ca^{2+} removal rate in carboxyeosin + CPA (R_{CE+CPA}) across the range of Ca^{2+} measured. *C*: sample trace showing train-evoked Ca^{2+} influx and removal with high external pH (pH = 8.8) to inhibit the PMCA (light trace). In high external pH, CPA does not change the peak Ca^{2+} influx or Ca^{2+} removal elicited by the train (dark trace). TPP is included in both experimental conditions. *D*: in the presence of carboxyeosin (*left*) or high external pH (pH = 8.8) (*right*), CPA does not significantly alter the posttrain area (unpaired Student's *t*-test for both).

extracellular alkalization was used to inhibit Ca^{2+} removal via the PMCA; again, 100 μM TPP was present to prevent CICR. Cells exposed to both high external pH and 20 μM CPA (n = 5) showed a posttrain Ca^{2+} decay period that was comparable to high external pH alone (n = 6) (Fig. 6*C*). In high external pH, CPA did not significantly change the posttrain area above baseline (Fig. 6*D*, *right*).

PMCA, Mitochondria, and ER Localize to Regions of Voltage-Gated Ca^{2+} Influx in Soma

That the PMCA and mitochondria influence activity-dependent Ca^{2+} dynamics in the bag cell neurons suggests that these Ca^{2+} handling systems are prevalent near sites of voltage-gated Ca^{2+} entry in the soma. To address this, we examined the spatial pattern of voltage-gated Ca^{2+} influx and compared it with the somatic distribution of the PMCA and mitochondria in cultured bag cell neurons. Initially, the spatial pattern of voltage-gated Ca^{2+} entry was assessed by inspecting ratiometric Ca^{2+} images before and during the 5-Hz, 1-min train from H_2O- or DMSO-treated control neurons presented in Fig. 2*D* and Fig. 4*B*. In all neurons (n = 19), images from the midpoint of the vertical somatic focal plane showed that intracellular Ca^{2+} was low and homogeneous throughout the soma at rest (Fig. 7*A*, *inset 1*). Shortly after the stimulus onset, Ca^{2+} increased first at the soma periphery (Fig. 7*A*, *inset 2*). As the stimulus progressed, Ca^{2+} in the center of the soma increased to similar levels as the periphery, likely as a result of Ca^{2+} diffusion from the plasma membrane (Fig. 7*A*, *insets 3* and *4*).

The distribution of the PMCA was then determined by immunolabeling fixed cultured bag cell neurons (n = 18) with a mouse antibody raised against an epitope of the human PMCA (1:200 mouse anti-PMCA; 1:200 goat anti-mouse Alexa Fluor 594). This epitope is strongly conserved in a putative *Aplysia* PMCA homologue (see *Live-Cell Staining, Immunocytochemistry, and Immunohistochemistry* for details). Considering the influence of the PMCA on the handling of Ca^{2+} from voltage-gated Ca^{2+} channels, we expected abundant membrane staining. To discern this, confocal microscopy was used to view PMCA immunolabeling in the midsomatic focal plane. Horizontal and vertical optical sections through the center of the soma revealed that, although fluorescent signal was certainly present throughout, the near-membrane region contained the greatest immunolabeling intensity, consistent with the plasma membrane localization of the PMCA (Fig. 7, *B–D*). Vertical optical sections also showed PMCA immunolabeling in most portions at or near the somatic membrane, with slightly more abundance in the left and right portions than the upper and bottom poles (Fig. 7, *C* and *D*).

To label and view the distribution of mitochondria in living cultured cells, we stained with MitoTracker Red (500 nM in DMSO), a vital dye used previously for this purpose in bag cell neurons (Groten and Magoski 2015; White and Kaczmarek 1997) (n = 11). Horizontal and vertical confocal microscopy optical sections through the center of the soma revealed that the mitochondria were present both peripherally, near the plasma membrane, and in central cytosolic regions (Fig. 7, *E–G*). The staining pattern in the soma often appeared reticular in arrangement. This morphology bears likeness to the "mitochondrial networks" present in other cell types (MacAskill and Kittler 2010; Rizzuto et al. 1998). Furthermore, in 7 of 11 cells, vertical optical sections revealed a large, dense core of mitochondrial labeling spanning from the perinuclear region to the upper portion of the cytosol above the nucleus (Fig. 7, *F* and *G*).

The present study, as well as our prior work (Groten et al. 2013), suggests that, unlike the mitochondria, the ER is seemingly not involved in the removal of Ca^{2+} from voltage-gated influx. A possible explanation for this is a difference in the distribution or abundance of the ER relative to sources of voltage-gated Ca^{2+} entry. To address this, a rat anti-KDEL antibody (1:200 anti-KDEL; 1:200 goat anti-rat Alexa Fluor 488) was used to immunolabel the ER in fixed cultured neurons (n = 12). KDEL (Lys-Asp-Glu-Leu) is a highly conserved ER-retention signal found in the COOH terminus of proteins localized to the ER (Munro and Pelham 1987), including those of *Aplysia* (Kennedy et al. 1992). Also, this antibody has been employed previously to identify ER in cultured *Aplysia* sensory neurons and bag cell neurons (Lyles et al. 2006; Zhang and Forscher 2009). Interestingly, confocal microscopy horizontal optical sections revealed that the ER was abundant near the soma periphery, where voltage-gated Ca^{2+} influx is observed (Fig. 7*H*). However, this positioning at the membrane was not consistent throughout all portions of the soma. In contrast to the mitochondria, vertical optical sections revealed that the ER was polarized to select divisions of the soma. Specifically, the upper and bottom poles of the somatic membrane region, where mitochondria are prevalent, were comparatively devoid of ER (Fig. 7, *I* and *J* vs. *F* and *G*).

To assess regional differences in their distribution, PMCA, mitochondria, and ER fluorescence intensities were quantified from regions of interest in the left, right, upper, and bottom poles of the soma (see *Live-Cell Staining, Immunocytochemistry, and Immunohistochemistry* for details) (Fig. 7*K*). Although PMCA immunolabeling was present in the upper and bottom regions, it was less abundant here compared with the left, but not the right, region. Mitochondrial staining was essentially the same across all regions of the soma periphery; furthermore, there were no differences in the distribution of the PMCA vs. the mitochondria, except for the left region of PMCA labeling being greater than the left region of mitochondrial staining. Immunolabeling of the ER was not different between the left and right regions or the upper and bottom regions; however, these two groups were collectively different from each other. In addition, the signal from the upper and bottom regions for ER was less than the majority of the regions labeled for the PMCA or mitochondria. Specifically, immunolabeling of the ER in the upper region was smaller than the left and right regions of PMCA immunolabeling, along with the upper, bottom, and right regions of mitochondrial staining, while signal from the bottom region for ER was less compared with all regions of PMCA or mitochondria labeling. Finally, the right region of ER immunolabeling was greater than the upper and bottom regions of PMCA immunolabeling, as well as the left region of mitochondrial staining.

Even with competition for Ca^{2+} removal by the PMCA disrupted, the ER was not shown to influence the removal of Ca^{2+} from voltage-gated Ca^{2+} channels. This may suggest that the areas of the plasma membrane containing the PMCA are not associated with regions of the ER that approach the somatic plasma membrane. We examined this by assessing the colocalization between peripheral ER and PMCA in single cultured

neurons with double labeling with anti-PMCA and anti-KDEL ($n = 15$). Horizontal confocal optical sections revealed that the ER (*x,y* image of Fig. 7*L*) and PMCA (*x,y* image of Fig. 7*M*) are present in similar regions of the periphery, particularly in the left and right portions of the soma. However, vertical cross sections revealed that this regional similarity was less apparent at the upper and bottom poles, where the PMCA, but not the ER, is present (*x,z* and *y,z* images of Fig. 7*L* vs. Fig. 7*M*). Merging the KDEL and PMCA immunocytochemical images distinctly showed a more restricted ER labeling compared with the PMCA (*x,z* and *y,z* images of Fig. 7*N*).

As culture conditions can influence the morphology of bag cell neurons (Gruenbaum and Carew 1999), it is possible that the distribution of the ER in the soma is altered in vitro relative to the cluster in the abdominal ganglion. This may explain why we found that the distribution of the ER differed in relation to the site of cell attachment on the glass coverslip. To examine this prospect, cryostat horizontal sections of bag cell neuron clusters in the abdominal ganglion were immunolabeled with anti-KDEL to stain the ER ($n = 6$ clusters from 3 animals). Unsurprisingly, the ER was present in bag cell neurons within the cluster (Fig. 8, *A*, *left*, and *B*, *left*). For individual neurons, the ER was abundant throughout the soma, and like the in vitro conditions it frequently formed dense appositions near the plasma membrane (Fig. 8*A*, *right*, and *B*, *right*). That stated, the markedly heterogeneous distribution seen in cultured bag cell

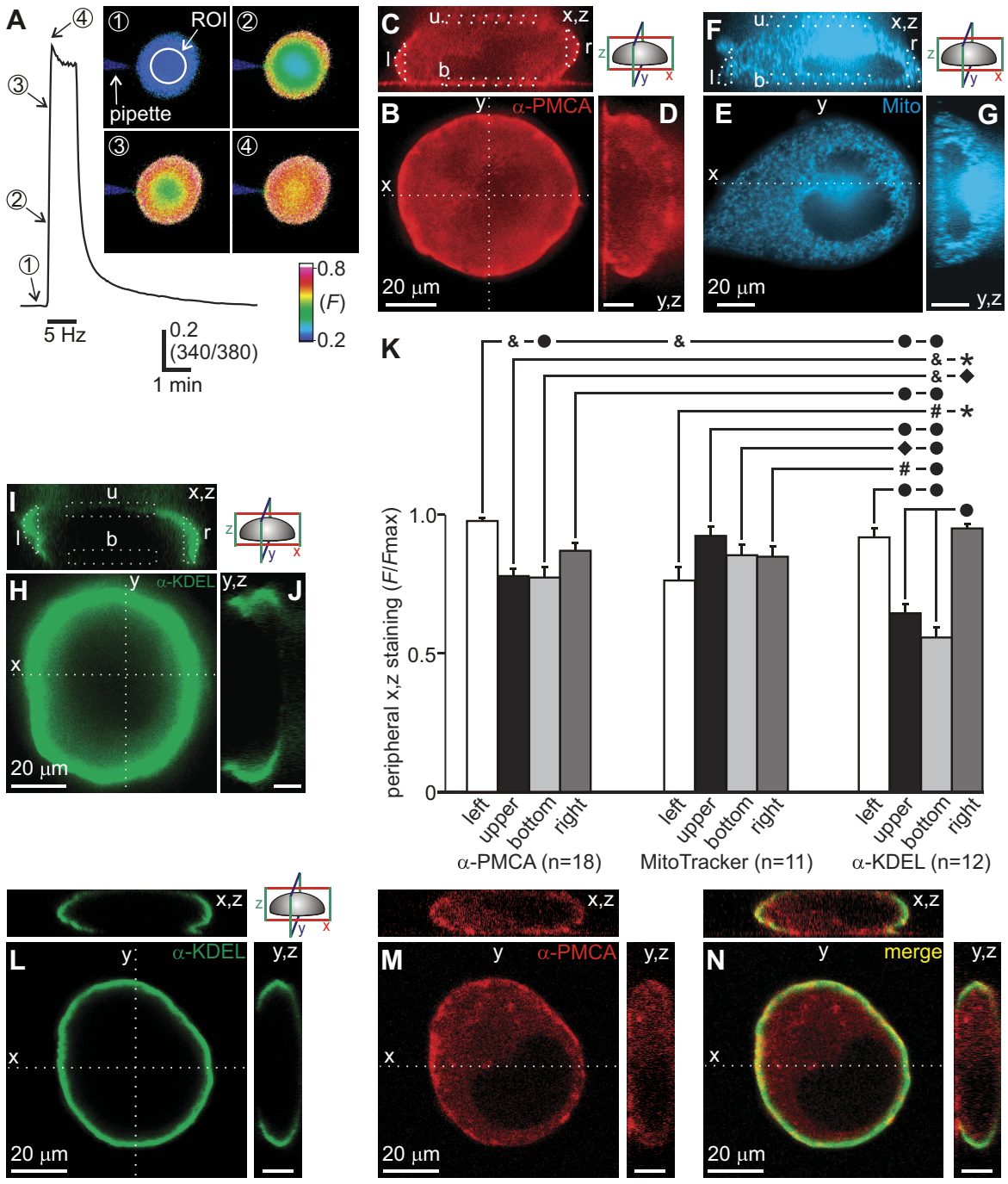

neurons, where the ER was concentrated along the sides of the cell, was less pronounced in the cluster (compare to Fig. 7, *H–J* and *L*). To explore this in detail, we examined the ER distribution in individual bag cell neurons that were clearly identifiable across neighboring cyrosections. In six different cases, one or more immunolabeled neurons could be recognized in consecutive serial sections; two examples are provided in Fig. 8, *C–H*. These instances revealed that while the ER was evident near the plasma membrane it was also distributed within the cytoplasm along the dorso-ventral axis of single bag cell neurons in the cluster.

DISCUSSION

The present study demonstrates that Ca^{2+} removal by the PMCA influences the threshold of stimulation required to elicit CICR. Evidence for this comes from our finding that inhibiting Ca^{2+} removal by the PMCA rescues train-evoked CICR in cells recorded with EGTA-containing intracellular solution. That stated, we realize that the increased Ca^{2+} buffering capacity provided by EGTA definitely impacts the ability of PMCA inhibition to bring back CICR. Nevertheless, even in the absence of intracellular EGTA, antagonizing the PMCA with carboxyeosin allows for apparent CICR following a stimulus that is typically subthreshold for initiating the response. This is consistent with other neuronal types, where a steep relationship between the extent of Ca^{2+} influx and the magnitude of intracellular Ca^{2+} release has been identified. For example, in bullfrog sympathetic neurons, CICR grows dramatically with longer depolarizing stimuli (Colegrove et al. 2000a, 2000b; Friel and Tsien 1994). Likewise, in dorsal root ganglion neurons, augmented Ca^{2+} influx, mediated by the insertion of additional plasma membrane Ca^{2+} channels, causes the appearance of mitochondrial CICR to a normally ineffective depolarizing stimulus (D'Arco et al. 2015).

The strong dependence of CICR on intracellular Ca^{2+} has been attributed to the properties of the MCU, which underlies mitochondrial Ca^{2+} uptake and, in turn, the level of subsequent Ca^{2+} release. Although the uniporter only opens after intracellular Ca^{2+} is elevated considerably by voltage-gated influx, once engaged uptake occurs with great capacity over a large range of Ca^{2+} concentrations (Herrington et al. 1996; Kirichok et al. 2004). Importantly, the passage of Ca^{2+} through the mitochondrial uniporter increases in a nonlinear fashion with cytosolic Ca^{2+} (Gunter and Pfeiffer 1990; Herrington et al. 1996; Kirichok et al. 2004; Mallilankaraman et al. 2012; Patron et al. 2014; Perocchi et al. 2010). Consequently, slight changes in cytosolic Ca^{2+} can profoundly alter both the scale of Ca^{2+} uptake and ensuing Ca^{2+} release.

In this respect, the magnitude of Ca^{2+} efflux by the PMCA could in effect gate CICR by influencing the availability of Ca^{2+} for uptake by the mitochondria (Fig. 9). Carboxyeosin heightens the sensitivity of posttrain Ca^{2+} removal to FCCP, a finding consistent with an augmented role of the mitochondria in the removal of Ca^{2+} following voltage-gated Ca^{2+} influx. Furthermore, our physiological data and a Ca^{2+} compartment model demonstrate that the extent to which the mitochondria take up the Ca^{2+} entering through voltage-gated channels is increased when the PMCA is inhibited. The influence of Ca^{2+} removal by the PMCA on mitochondrial Ca^{2+} uptake and release is consistent with their apparent distribution in the bag cell neurons. Immunocytochemistry and live cell staining sug-

[1] Supplemental Material for this article is available online at the Journal website.

Fig. 7. The PMCA, mitochondria, and ER are present near regions of voltage-gated Ca^{2+} influx in the soma. *A*: intracellular Ca^{2+} of a cultured bag cell neuron during the 5-Hz, 1-min train. *Insets*: ratiometric fura images of a neuron obtained with conventional fluorescence microscopy from the midpoint of the vertical somatic focal plane; the recording pipette and the region of interest (ROI) for data acquisition are indicated. Images are from the time points numbered on the sample trace. *Inset 1*, before stimulation, intracellular Ca^{2+} is low and homogeneous throughout the soma. *Inset 2*, shortly after the train onset, a rise in intracellular Ca^{2+} is apparent at the soma periphery. *Insets 3* and *4*, as the stimulus progresses, intracellular Ca^{2+} appears to propagate from the periphery toward the middle of the soma. *B*: representative 1-μm horizontal optical section (*x*-, *y*-axes) gathered by confocal microscopy at the midpoint of the vertical (*z*-axis) focal plane shows PMCA immunolabeling (1:200 anti-PMCA 1°; 1:200 Alexa Fluor 594 2°) of a fixed cultured bag cell neuron. PMCA immunolabeling is most abundant in association with the plasma membrane. Scale bar also applies to *C*. *C* and *D*: vertical (*z*-axis) cross sections dissect the cell into slices along the *x* (*C*) and *y* (*D*) planes. PMCA immunolabeling is present in most near-membrane regions, including the left (l), right (r), upper (u; away from the glass coverslip), and bottom (b; toward the glass coverslip) portions of the soma. Outlined regions denote the ROI used to quantify peripheral staining (see *Live-Cell Staining, Immunocytochemistry, and Immunohistochemistry* for details) Scale bar, 20 μm. *E*: a live cultured bag cell neuron labeled with MitoTracker Red (500 nM in DMSO) to stain mitochondria. Confocal images are pseudocolored blue to avoid confusion with the red PMCA immunolabeling in *B–D*. Representative 1-μm horizontal optical section (*x*-, *y*-axes) from halfway up the *z*-axis shows mitochondrial labeling. Mitochondria are distributed peripherally, near the plasma membrane, and in the cytosol surrounding the nucleus. Scale bar also applies to *F*. *F* and *G*: vertical (*z*-axis) cross sections dissect the cell along the *x* (*F*) and *y* (*G*) planes. Mitochondria are present throughout the cell and form a dense core above the nucleus. Scale bar, 20 μm. *H*: a fixed cultured bag cell neuron immunolabeled with α-KDEL to visualize the ER (1:200 anti-KDEL 1°; 1:200 Alexa Fluor 488 2°). Confocal image shows a 2-μm horizontal (*x,y* plane) cross section of ER staining at mid-*z*-axis. The ER is present in greatest proportion near the soma periphery. Scale bar also applies to *I*. *I* and *J*: vertical (*z*-axis) cross sections dissect the cell into *x* (*I*) and *y* (*J*) planes. ER is highly polarized toward the left and right regions, with substantially less in the upper and bottom portions. Scale bar, 20 μm. *K*: summary data showing the relative PMCA immunolabeling, mitochondrial MitoTracker staining, and KDEL/ER immunolabeling in the upper, bottom, left, and right regions in the *x,z* plane of the soma periphery. Fluorescence is normalized by dividing each ROI by the ROI with the greatest fluorescence in a given neuron (F/F_{max}). Differences in labeling are apparent within and between the 3 groups ($F_{11,156} = 13.88$, $P < 0.0001$, 1-way ANOVA; $^{*}P < 0.02$, $^{\bullet}P < 0.01$, $^{\#}P < 0.005$, $^{\blacktriangle}P < 0.004$, $^{\&}P < 0.001$, $^{\bullet}P < 0.0001$, Tukey's post hoc test adjusted for multiple comparisons; see Supplemental Table S1 for the details of all statistical comparisons).[1] PMCA labeling in the left region of the soma is significantly greater than in the upper and bottom regions but not the right. Any differences in mitochondrial labeling between regions fail to reach significance; however, the left region labeled for mitochondria is significantly less than the left region of PMCA labeling. ER labeling reveals that the left and right regions, while not significantly different from one another, are significantly greater than the upper and bottom regions. Also, labeling of ER in the upper region is significantly less than in the left and right regions of PMCA labeling, along with the upper, bottom, and right regions of mitochondrial labeling. Furthermore, ER labeling in the bottom region is significantly less compared with all regions of PMCA or mitochondria labeling. Finally, the right region of ER labeling is significantly greater than the upper and bottom regions of PMCA labeling, along with the left region of mitochondrial labeling. *L* and *M*: horizontal (1-μm width, *x,y*) and vertical (*x,z* and *y,z*) confocal sections of a cultured bag cell neuron double-labeled with anti-KDEL and anti-PMCA. *N*: overlay of the horizontal optical sections for anti-KDEL and anti-PMCA shows similarity in the distribution of the ER and PMCA at the soma periphery. Vertical cross sections in the *x,z* and *y,z* planes show that the ER and PMCA are both found in the middle portions of the soma, but this similarity is less obvious at the upper and bottom poles, where the PMCA, but not the ER, is more abundant.

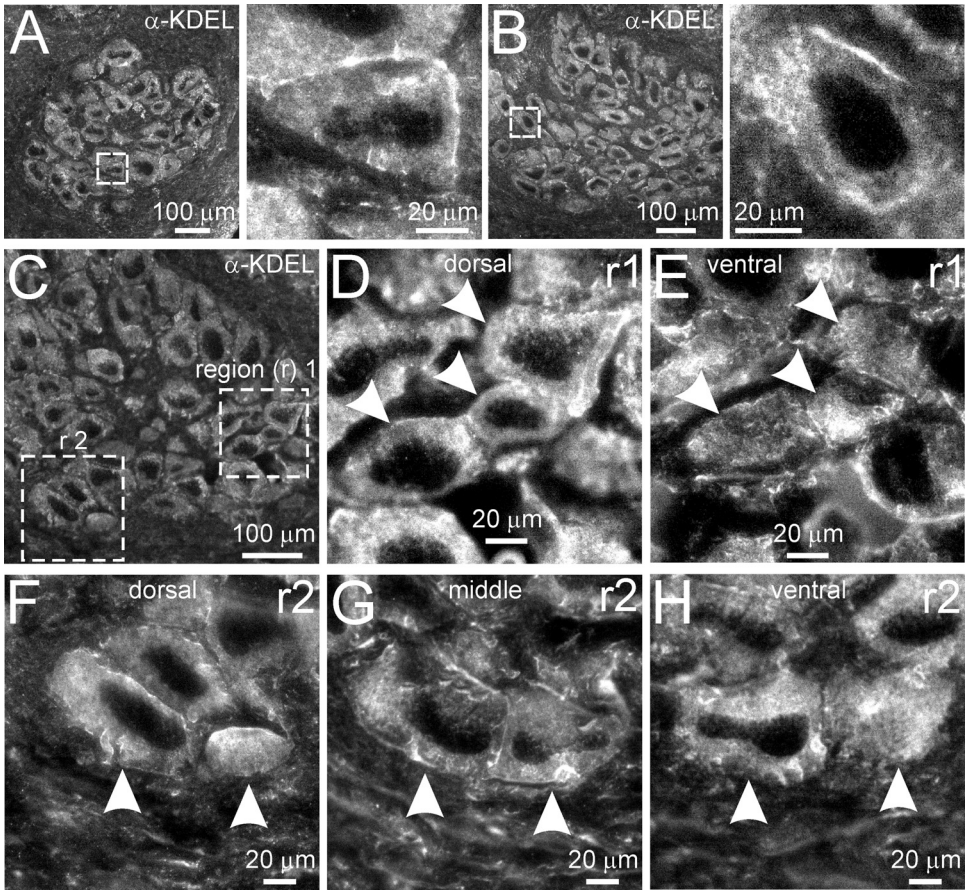

Fig. 8. In the bag cell neuron cluster, the ER is particularly abundant at the soma periphery but is also present in other cellular regions. *A*: images of ER immunolabeling (α-KDEL 1° at 1:200; Alexa Fluor 488 2° at 1:200) in 6-μm thick tissue sections of the abdominal ganglion (see *Live-Cell Staining, Immunocytochemistry, and Immunohistochemistry* for details). *Left*: photomicrograph of a cluster of bag cell neurons and surrounding tissue. White dashed box outlines the region magnified at *right*. *Right*: higher-magnification image showing ER labeling in the soma of a single bag cell neuron. The ER is present throughout the soma but is particularly abundant near the membrane. *B*: another bag cell neuron cluster (*left*), where strong peripheral labeling is apparent in the soma of the outlined cell (magnified at *right*). *C*: serial neighboring tissue sections (6 μm thick) from a single bag cell neuron cluster along the dorso-ventral axis. Rectangles delineate 2 regions (*r1* and *r2*) of the cluster where neurons were identifiable across neighboring tissue sections. *D* and *E*: magnified images of *region r1* from *C*. Arrowheads point to 2 neurons that are identifiable in serial neighboring sections. *D* and *E* are dorsal and ventral regions of the abdominal ganglion, respectively, and ER labeling is apparent in neurons from both sections. *F–H*: magnified images of *region r2* from *C*. Arrowheads point to 3 neurons that are identifiable across 3 neighboring sections in the dorso-ventral axis: dorsal (*F*), middle (*G*), and ventral (*H*). In all 3 sections, the ER is abundant throughout each bag cell neuron.

gest that at the somatic plasma membrane, where voltage-gated Ca^{2+} influx occurs, the PMCA and mitochondria are relatively abundant with essentially similar distributions (although mitochondria are most concentrated in the central regions of the soma). Consequently, the PMCA appears ideally positioned to remove Ca^{2+} entry across the plasma membrane and limit the availability of Ca^{2+} for uptake by the mitochondria.

An interplay between Ca^{2+} removal systems and mitochondrial Ca^{2+} uptake has been characterized in other neurons. In the synaptic terminals of goldfish retinal bipolar neurons, the PMCA is the principal handling system for Ca^{2+} arising from voltage-gated influx, while the mitochondria are typically uninvolved (Zenisek and Matthews 2000). However, after disrupting the PMCA, the mitochondria then participate in the removal of Ca^{2+} from voltage-gated Ca^{2+} channels (Zenisek and Matthews 2000). Likewise, in the rat calyx of Held, Ca^{2+} removal by the plasma membrane Na^+/Ca^{2+} exchanger influences the amount of mitochondrial Ca^{2+} uptake (Kim et al. 2005). In doing so, it was shown that developmental changes in Na^+/Ca^{2+} exchanger expression at this synapse dictate the appearance of posttetanic mitochondrial Ca^{2+} release (Lee et al. 2013). Interestingly, compared with these other neuronal systems, bag cell neuron CICR occurs as a result of augmented mitochondrial Ca^{2+} uptake and is much more apparent. This may be explained by the fact that Ca^{2+} removal in the bag cell neurons has a greater dependence on mitochondrial Ca^{2+} uptake than in other neurons, as indicated by the sensitivity of posttrain Ca^{2+} handling to FCCP even when the PMCA is active (Geiger and Magoski 2008; Groten et al. 2013).

It appears that the PMCA does not play a large role in handling Ca^{2+} entering at rest, given that we found no difference in basal Ca^{2+} levels between control and carboxyeosin or high external pH. A contributing factor might be the relatively small resting Ca^{2+} influx across the bag cell neuron plasma membrane (Geiger et al. 2009). With a small Ca^{2+} leak, there may be little Ca^{2+} for the PMCA to handle at rest, and as a result any effect of inhibiting the PMCA on resting Ca^{2+} would not be easily detected. Also, any Ca^{2+} that becomes available after PMCA inhibition may be quickly removed by other buffering systems, such as the mitochondria.

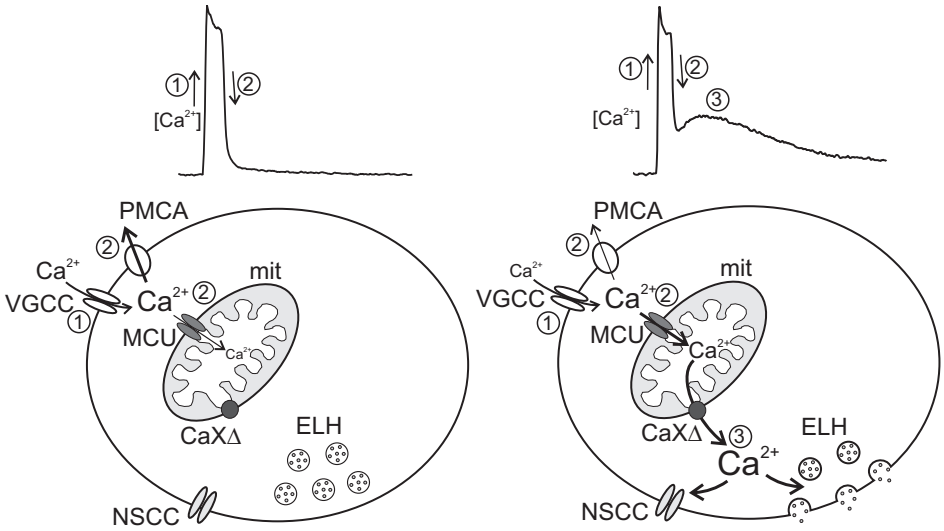

Fig. 9. The interplay between the PMCA and mitochondria determines the removal of Ca^{2+} from voltage-gated influx and the presence of CICR in the bag cell neurons: conceptual model of activity-dependent Ca^{2+} dynamics in the bag cell neurons under whole cell recording conditions based on the present study and prior work by our laboratory and others (Geiger and Magoski 2008; Groten and Magoski 2015; Hickey et al. 2010, 2013; Hung and Magoski 2007; Michel and Wayne 2002; Wayne et al. 1998). *Left*: sample trace (*top*) of intracellular Ca^{2+} in response to a fast-phase period of activity when the PMCA is fully active. Numbers correspond to the chronology portrayed in the illustration: *1*, voltage-gated Ca^{2+} channels (VGCC) open and allow Ca^{2+} to enter the cytosol; *2*, subsequently, intracellular Ca^{2+} is removed by plasma membrane Ca^{2+} extrusion with the PMCA and mitochondrial Ca^{2+} uptake via the mitochondrial Ca^{2+} uniporter (MCU). The PMCA limits the Ca^{2+} available for uptake into the mitochondria and, in turn, prevents CICR from the mitochondria. *Right*: sample trace (*top*) showing intracellular Ca^{2+} during fast-phase activity when Ca^{2+} extrusion by the PMCA is diminished: *1*, the activation of voltage-gated Ca^{2+} channels causes Ca^{2+} influx into the cytosol; *2*, reduced Ca^{2+} extrusion by the PMCA increases the availability of Ca^{2+} for uptake by the mitochondria; *3*, the greater Ca^{2+} load results in Ca^{2+} extrusion out of the mitochondria (CaXΔ) and thereby prolongs the initial influx signal. Such Ca^{2+} release could elicit egg-laying hormone (ELH) secretion and activate Ca^{2+}-dependent nonselective cation channels (NSCC) to increase membrane excitability.

Although our results indicate that the influence of Ca^{2+} handling by the PMCA on Ca^{2+} uptake and release occurs primarily through its effects on cytosolic Ca^{2+}, different mechanisms must also be considered. In other neurons, reducing PMCA activity has been shown to prevent the transient extracellular alkalization and intracellular acidification that arise from its proton transport ability (Makani and Chesler 2010; Niggli et al. 1982; Thomas 2011). Such changes can modulate the function of several ion channels (Chen and Chesler 2015), including voltage-gated Ca^{2+} channels (Zhou and Jones 1996), or influence the pH-dependent processes required for mitochondrial Ca^{2+} uptake and H^+/Ca^{2+} exchanger-mediated Ca^{2+} release (Jiang et al. 2009; Santo-Domingo and Demaurex 2010). That stated, it is doubtful that the activation of the PMCA during voltage-gated Ca^{2+} influx has a substantial effect on intracellular pH in the present study, as prior work has shown that Ca^{2+} derived from other channels does not alter the acidity of the cytosol (Knox et al. 2004). Even if such changes occurred, it is unlikely that disrupting proton transport by the PMCA would enhance bag cell neuron CICR by modulating voltage-gated Ca^{2+} channels or mitochondrial Ca^{2+} release. Carboxyeosin should preclude extracellular alkalization by the PMCA (Makani and Chesler 2010), a property that would prevent any alkaline shift-dependent enhancement of Ca^{2+} current (Zhou and Jones 1996). Indeed, our measurements of intracellular Ca^{2+} show that train-evoked Ca^{2+} influx was slightly smaller in carboxyeosin and high external pH. Both mitochondrial Ca^{2+} uptake and H^+/Ca^{2+}-mediated release increase with intracellular acidification (Jiang et al. 2009; Santo-Domingo and Demaurex 2010). Thus carboxyeosin or high external pH, which would prevent any potential PMCA-dependent intracellular acidification, should decrease, not increase, mitochondrial Ca^{2+} uptake and release. Consequently, the effects of the PMCA on stimulus-evoked Ca^{2+} dynamics can be most parsimoniously attributed to its influence on Ca^{2+} transport across the plasma membrane.

A noteworthy result from our study was that, unlike the mitochondria, the ER appears uninvolved in the removal of Ca^{2+} from voltage-gated influx, even when Ca^{2+} handling by the PMCA is disrupted. This contrasts with some neurons in other species, where both the ER and mitochondria have a role in Ca^{2+} removal (Fierro et al. 1998; Kim et al. 2003; Wheeler et al. 2012). Like other neurons (McDonough et al. 2000; Wheeler et al. 2012), we find that the ER in bag cell neurons forms dense appositions near the soma periphery both in vitro and in the cluster. These structures may represent subsurface cisternae, stacks of densely packed ER membrane that function in highly compartmentalized Ca^{2+} signaling (Berridge 1998). Indeed, freeze-fracture sections of bag cell neuron clusters reveal an array of ER membrane, resembling subsurface cisternae, that is often opposed to the somatic plasma membrane (Kaczmarek et al. 1979). Considering that the ER in the soma periphery is closely associated with sites of voltage-gated Ca^{2+} influx and the PMCA, it is surprising that the organelle does not contribute to Ca^{2+} removal, even when the PMCA is inhibited. However, given that our Ca^{2+} measurements reflect the average Ca^{2+} signal from the entire soma, and considering that the mitochondria, but not the ER, are found throughout the cell, it may be reasonable to expect that Ca^{2+} handling by the mitochondria would be more readily detected than that by the ER. Furthermore, the SERCA is known to be comparatively high-affinity, low-capacity relative to the mitochondria, while the MCU is often considered a low-affinity, high-capacity uptake system (Berridge 1998; Herrington et al. 1996;

Werth and Thayer 1994). Consequently, it is likely that the ER contributes only in a small manner to remove Ca^{2+} from voltage-gated influx, and this is largely undetectable over the time periods we observed.

The relative abundance of the ER and mitochondria in the soma may contribute to the preeminence of mitochondrial Ca^{2+} handling. In cultured neurons, the localization of the ER is polarized, with less of a concentration in the lower and upper regions of the soma periphery compared with both the left and right regions, as well as the majority of regions for both the PMCA and the mitochondria. Also, a greater prevalence of mitochondria in the center of the soma may confer an advantage to these organelles in removing Ca^{2+} entering via voltage-gated channels. However, it should be noted that the apparent lack of ER involvement could be a by-product of the cell culture conditions, as the organelle is more homogeneously distributed in bag cell neurons in the cluster than in vitro. This may reflect the influence of cell-to-cell and cell-to-extracellular matrix interactions on how the ER is localized in the cluster compared with in vitro. Also, for cultured neurons the attachment to the culture dish, as well as the lack of attachment at the top of the cell, could restrict the ER from those areas. Finally, there are some apparent differences in somatic distribution that may not be all that biologically meaningful, for example, the disparity between the ER in the right region and mitochondria in the left region, or the amount of PMCA vs. mitochondria in the left regions. Ostensibly, these findings are largely the function of the left mitochondrial staining being, inexplicably, slightly low.

A growing body of evidence has established that plasma membrane Ca^{2+} extrusion by either the PMCA or Na^+/Ca^{2+} exchanger can modify activity-dependent processes, including short-term presynaptic plasticity, long-term potentiation, and afterhyperpolarizations (Empson et al. 2007; Ghosh et al. 2011; Jensen et al. 2007; Jeon et al. 2003). These findings have been primarily attributed to the ability of Ca^{2+} handling systems to control the rate at which Ca^{2+} from voltage-gated influx is removed. In many neurons, intracellular Ca^{2+} release promotes activity-dependent changes in excitability and synaptic transmission (Garcia-Chacon et al. 2006; Lee et al. 2007; Tang and Zucker 1997). Consequently, our research indicates that Ca^{2+} removal systems could control neuronal plasticity by regulating CICR. Evidence for this comes from the calyx of Held, where changes in Na^+/Ca^{2+} exchanger expression are shown to gate the presence of posttetanic potentiation by controlling the magnitude of mitochondrial Ca^{2+} uptake and release (Kim et al. 2005; Lee et al. 2013).

In this respect, the ability of Ca^{2+} removal by the PMCA to influence CICR may have important consequences for bag cell neuron afterdischarge and reproductive behavior (Fig. 9). CICR is initiated during the bag cell neuron in the intact cluster (Fisher et al. 1994) and is implicated in sustaining peptide secretion, as some prior studies show that a substantial amount of egg-laying hormone release during the afterdischarge occurs independent of extracellular Ca^{2+} (Michel and Wayne 2002; Wayne et al. 1998). Because the mitochondrial Ca^{2+} store is a principal source of CICR in the bag cell neurons, it may contribute to peptide secretion during the afterdischarge (Geiger and Magoski 2008; Groten et al. 2013). Aside from secretion, mitochondrial Ca^{2+} release also activates nonselective cation currents (Hickey et al. 2010), which provide the depolarizing drive that sustains the afterdischarge (Hung and Magoski 2007; Wilson et al. 1996).

Mitochondrial Ca^{2+} release is implicated in several crucial events during the afterdischarge; thus our present findings suggest that the modulation of PMCA activity could potently change the propensity for CICR and its downstream effectors. However, because the effect of the PMCA on CICR was demonstrated pharmacologically, it is not clear whether this occurs in response to physiological changes in PMCA function. Interestingly, in other preparations, the contribution of plasma membrane Ca^{2+} extrusion by the PMCA can be modified by pretranslational mechanisms, as well as protein kinases known to be engaged during the afterdischarge (Ghosh et al. 2011; Kaczmarek et al. 1978; Lee et al. 2013; Magoski and Kaczmarek 2005; Usachev et al. 2002; Wang et al. 1992; Wayne et al. 1999; Zacharias and Strehler 1996). It may be that physiological changes in PMCA function occur in the bag cell neurons to influence activity-dependent Ca^{2+} dynamics.

ACKNOWLEDGMENTS

The authors thank Dr. C. J. Carter for the *in silico* identification of the *Aplysia californica* PMCA and Dr. K. Ding for advice on statistical analysis.

GRANTS

This work was supported by a Canadian Institutes of Health Research operating grant to N. S. Magoski. C. J. Groten held an National Sciences and Engineering Research Council Post-graduate Doctoral Scholarship.

DISCLOSURES

No conflicts of interest, financial or otherwise, are declared by the author(s).

AUTHOR CONTRIBUTIONS

C.J.G., J.T.R., G.B., and N.S.M. conception and design of research; C.J.G., J.T.R., H.M.H., and A.K.C. performed experiments; C.J.G., J.T.R., and H.M.H. analyzed data; C.J.G., J.T.R., G.B., and N.S.M. interpreted results of experiments; C.J.G. and J.T.R. prepared figures; C.J.G. drafted manuscript; C.J.G. and N.S.M. edited and revised manuscript; C.J.G., J.T.R., H.M.H., A.K.C., G.B., and N.S.M. approved final version of manuscript.

REFERENCES

Arch S. Polypeptide secretion from the isolated parietovisceral ganglion of *Aplysia californica*. *J Gen Physiol* 59: 47–59, 1972.

Babcock DF, Herrington J, Goodwin PC, Park YB, Hille B. Mitochondrial participation in the intracellular Ca^{2+} network. *J Cell Biol* 136: 833–844, 1997.

Baughman JM, Perocchi F, Girgis HS, Plovanich M, Belcher-Timme CA, Sancak Y, Bao XR, Strittmatter L, Goldberger O, Bogorad RL, Koteliansky V, Mootha VK. Integrative genomics identifies MCU as an essential component of the mitochondrial calcium uniporter. *Nature* 476: 341–345, 2011.

Berridge MJ. Neuronal calcium signaling. *Neuron* 21: 13–26, 1998.

Berridge MJ. The endoplasmic reticulum: a multifunctional signaling organelle. *Cell Calcium* 32: 235–249, 2002.

Blaustein MP, Lederer WJ. Sodium/calcium exchange: its physiological implications. *Physiol Rev* 79: 763–854, 1999.

Carafoli E, Genazzani A, Guerini D. Calcium controls the transcription of its own transporters and channels in developing neurons. *Biochem Biophys Res Commun* 266: 624–632, 1999.

Carafoli E, Tiozzo R, Lugli G, Crovetti F, Kratzing C. The release of calcium from heart mitochondria by sodium. *J Mol Cell Cardiol* 6: 361–371, 1974.

Chen HY, Chesler M. Autocrine boost of NMDAR current in hippocampal CA1 pyramidal neurons by a PMCA-dependent, perisynaptic, extracellular pH shift. *J Neurosci* 35: 873–877, 2015.

Chouhan AK, Ivannikov MV, Lu Z, Sugimori M, Llinas RR, Macleod GT. Cytosolic calcium coordinates mitochondrial energy metabolism with presynaptic activity. *J Neurosci* 32: 1233–1243, 2012.

Clapham DE. Calcium signaling. *Cell* 131: 1047–1058, 2007.

Colegrove SL, Albrecht MA, Friel DD. Dissection of mitochondrial Ca^{2+} uptake and release fluxes in situ after depolarization-evoked $[Ca^{2+}]_i$ elevations in sympathetic neurons. *J Gen Physiol* 115: 351–370, 2000a.

Colegrove SL, Albrecht MA, Friel DD. Quantitative analysis of mitochondrial Ca^{2+} uptake and release pathways in sympathetic neurons. Reconstruction of the recovery after depolarization-evoked $[Ca^{2+}]_i$ elevations. *J Gen Physiol* 115: 371–388, 2000b.

D'Arco M, Margas W, Cassidy JS, Dolphin AC. The upregulation of $\alpha_2\delta$-1 subunit modulates activity-dependent Ca^{2+} signals in sensory neurons. *J Neurosci* 35: 5891–5903, 2015.

Davies PJ, Ireland DR, McLachlan EM. Sources of Ca^{2+} for different Ca^{2+}-activated K^+ conductances in neurones of the rat superior cervical ganglion. *J Physiol* 495: 353–366, 1996.

Empson RM, Garside ML, Knopfel T. Plasma membrane Ca^{2+} ATPase 2 contributes to short-term synapse plasticity at the parallel fiber to Purkinje neuron synapse. *J Neurosci* 27: 3753–3758, 2007.

Fierro L, DiPolo R, Llano I. Intracellular calcium clearance in Purkinje cell somata from rat cerebellar slices. *J Physiol* 510: 499–512, 1998.

Fink LA, Connor JA, Kaczmarek LK. Inositol trisphosphate releases intracellularly stored calcium and modulates ion channels in molluscan neurons. *J Neurosci* 8: 2544–2555, 1988.

Fisher TE, Levy S, Kaczmarek LK. Transient changes in intracellular calcium associated with a prolonged increase in excitability in neurons of *Aplysia californica*. *J Neurophysiol* 71: 1254–1257, 1994.

Friel DD, Tsien RW. An FCCP-sensitive Ca^{2+} store in bullfrog sympathetic neurons and its participation in stimulus-evoked changes in $[Ca^{2+}]_i$. *J Neurosci* 14: 4007–4024, 1994.

Gabso M, Neher E, Spira ME. Low mobility of the Ca^{2+} buffers in axons of cultured *Aplysia* neurons. *Neuron* 18: 473–481, 1997.

Garcia-Chacon LE, Nguyen KT, David G, Barrett EF. Extrusion of Ca^{2+} from mouse motor terminal mitochondria via a Na^+-Ca^{2+} exchanger increases post-tetanic evoked release. *J Physiol* 574: 663–675, 2006.

Gardam KE, Geiger JE, Hickey CM, Hung AY, Magoski NS. Flufenamic acid affects multiple currents and causes intracellular Ca^{2+} release in *Aplysia* bag cell neurons. *J Neurophysiol* 100: 38–49, 2008.

Gatto C, Hale CC, Xu W, Milanick MA. Eosin, a potent inhibitor of the plasma membrane Ca pump, does not inhibit the cardiac Na-Ca exchanger. *Biochemistry* 34: 965–972, 1995.

Gatto C, Milanick MA. Inhibition of the red blood cell calcium pump by eosin and other fluorescein analogues. *Am J Physiol Cell Physiol* 264: C1577–C1586, 1993.

Geiger JE, Hickey CM, Magoski NS. Ca^{2+} entry through a non-selective cation channel in *Aplysia* bag cell neurons. *Neuroscience* 162: 1023–1038, 2009.

Geiger JE, Magoski NS. Ca^{2+}-induced Ca^{2+} release in *Aplysia* bag cell neurons requires interaction between mitochondrial and endoplasmic reticulum stores. *J Neurophysiol* 100: 24–37, 2008.

Ghosh B, Li Y, Thayer SA. Inhibition of the plasma membrane Ca^{2+} pump by CD44 receptor activation of tyrosine kinases increases the action potential afterhyperpolarization in sensory neurons. *J Neurosci* 31: 2361–2370, 2011.

Groten CJ, Magoski NS. PKC enhances the capacity for secretion by rapidly recruiting covert voltage-gated Ca^{2+} channels to the membrane. *J Neurosci* 35: 2747–2765, 2015.

Groten CJ, Rebane JT, Blohm G, Magoski NS. Separate Ca^{2+} sources are buffered by distinct Ca^{2+} handling systems in *Aplysia* neuroendocrine cells. *J Neurosci* 33: 6476–6491, 2013.

Gruenbaum LM, Carew TJ. Growth factor modulation of substrate-specific morphological patterns in *Aplysia* bag cell neurons. *Learn Mem* 6: 292–306, 1999.

Grynkiewicz G, Poenie M, Tsien RY. A new generation of Ca^{2+} indicators with greatly improved fluorescence properties. *J Biol Chem* 260: 3440–3450, 1985.

Gunter KK, Gunter TE. Transport of calcium by mitochondria. *J Bioenerg Biomembr* 26: 471–485, 1994.

Gunter TE, Pfeiffer DR. Mechanisms by which mitochondria transport calcium. *Am J Physiol Cell Physiol* 258: C755–C786, 1990.

Herrington J, Park YB, Babcock DF, Hille B. Dominant role of mitochondria in clearance of large Ca^{2+} loads from rat adrenal chromaffin cells. *Neuron* 16: 219–228, 1996.

Heytler PG, Prichard WW. A new class of uncoupling agents—carbonyl cyanide phenylhydrazones. *Biochem Biophys Res Commun* 7: 272–275, 1962.

Hickey CM, Geiger JE, Groten CJ, Magoski NS. Mitochondrial Ca^{2+} activates a cation current in *Aplysia* bag cell neurons. *J Neurophysiol* 103: 1543–1556, 2010.

Hickey CM, Groten CJ, Sham L, Carter CJ, Magoski NS. Voltage-gated Ca^{2+} influx and mitochondrial Ca^{2+} initiate secretion from *Aplysia* neuroendocrine cells. *Neuroscience* 250: 755–772, 2013.

Hung AY, Magoski NS. Activity-dependent initiation of a prolonged depolarization in *Aplysia* bag cell neurons: role for a cation channel. *J Neurophysiol* 97: 2465–2479, 2007.

Jensen TP, Filoteo AG, Knopfel T, Empson RM. Presynaptic plasma membrane Ca^{2+} ATPase isoform 2a regulates excitatory synaptic transmission in rat hippocampal CA3. *J Physiol* 579: 85–99, 2007.

Jeon D, Yang YM, Jeong MJ, Philipson KD, Rhim H, Shin HS. Enhanced learning and memory in mice lacking Na^+/Ca^{2+} exchanger 2. *Neuron* 38: 965–976, 2003.

Jiang D, Zhao L, Clapham DE. Genome-wide RNAi screen identifies Letm1 as a mitochondrial Ca^{2+}/H^+ antiporter. *Science* 326: 144–147, 2009.

Jobling P, McLachlan EM, Sah P. Calcium induced calcium release is involved in the afterhyperpolarization in one class of guinea pig sympathetic neurone. *J Auton Nerv Syst* 42: 251–257, 1993.

Jonas EA, Knox RJ, Smith TC, Wayne NL, Connor JA, Kaczmarek LK. Regulation by insulin of a unique neuronal Ca^{2+} pool and of neuropeptide secretion. *Nature* 385: 343–346, 1997.

Kachoei BA, Knox RJ, Uthuza D, Levy S, Kaczmarek LK, Magoski NS. A store-operated Ca^{2+} influx pathway in the bag cell neurons of *Aplysia*. *J Neurophysiol* 96: 2688–2698, 2006.

Kaczmarek LK, Finbow M, Revel JP, Strumwasser F. The morphology and coupling of *Aplysia* bag cells within the abdominal ganglion and in cell culture. *J Neurobiol* 10: 535–550, 1979.

Kaczmarek LK, Jennings K, Strumwasser F. Neurotransmitter modulation, phosphodiesterase inhibitor effects, and cyclic AMP correlates of afterdischarge in peptidergic neurites. *Proc Natl Acad Sci USA* 77: 7487–7491, 1978.

Kaczmarek LK, Jennings KR, Strumwasser F. An early sodium and a late calcium phase in the afterdischarge of peptide-secreting neurons of *Aplysia*. *Brain Res* 238: 105–115, 1982.

Karadjov JS, Kudzina LY, Zinchenko VP. TPP^+ inhibits Na^+-stimulated Ca^{2+} efflux from brain mitochondria. *Cell Calcium* 7: 115–119, 1986.

Kennedy TE, Kuhl D, Barzilai A, Sweatt JD, Kandel ER. Long-term sensitization training in *Aplysia* leads to an increase in calreticulin, a major presynaptic calcium-binding protein. *Neuron* 9: 1013–1024, 1992.

Kim MH, Korogod N, Schneggenburger R, Ho WK, Lee SH. Interplay between Na^+/Ca^{2+} exchangers and mitochondria in Ca^{2+} clearance at the calyx of Held. *J Neurosci* 25: 6057–6065, 2005.

Kim MH, Lee SH, Park KH, Ho WK, Lee SH. Distribution of K^+-dependent Na^+/Ca^{2+} exchangers in the rat supraoptic magnocellular neuron is polarized to axon terminals. *J Neurosci* 23: 11673–11680, 2003.

Kirichok Y, Krapivinsky G, Clapham DE. The mitochondrial calcium uniporter is a highly selective ion channel. *Nature* 427: 360–364, 2004.

Knox RJ, Jonas EA, Kao LS, Smith PJ, Connor JA, Kaczmarek LK. Ca^{2+} influx and activation of a cation current are coupled to intracellular Ca^{2+} release in peptidergic neurons of *Aplysia californica*. *J Physiol* 494.3: 627–639, 1996.

Knox RJ, Magoski NS, Wing D, Barbee SJ, Kaczmarek LK. Activation of a calcium entry pathway by sodium pyrithione in the bag cell neurons of *Aplysia*. *J Neurobiol* 60: 411–423, 2004.

Kupfermann I. Stimulation of egg laying: possible neuroendocrine function of bag cells of abdominal ganglion of *Aplysia californica*. *Nature* 216: 814–815, 1967.

Kupfermann I, Kandel ER. Electrophysiological properties and functional interconnections of two symmetrical neurosecretory clusters (bag cells) in abdominal ganglion of *Aplysia*. *J Neurophysiol* 33: 865–876, 1970.

Lee D, Lee KH, Ho WK, Lee SH. Target cell-specific involvement of presynaptic mitochondria in post-tetanic potentiation at hippocampal mossy fiber synapses. *J Neurosci* 27: 13603–13613, 2007.

Lee JS, Kim MH, Ho WK, Lee SH. Developmental upregulation of presynaptic NCKX underlies the decrease of mitochondria-dependent posttetanic potentiation at the rat calyx of Held synapse. *J Neurophysiol* 109: 1724–1734, 2013.

Llano I, DiPolo R, Marty A. Calcium-induced calcium release in cerebellar Purkinje cells. *Neuron* 12: 663–673, 1994.

Loechner KJ, Azhderian EM, Dreyer R, Kaczmarek LK. Progressive potentiation of peptide release during a neuronal discharge. *J Neurophysiol* 63: 738–744, 1990.

Lupinsky DA, Magoski NS. Ca^{2+}-dependent regulation of a non-selective cation channel from *Aplysia* bag cell neurones. *J Physiol* 575: 491–506, 2006.

Lyles V, Zhao Y, Martin KC. Synapse formation and mRNA localization in cultured *Aplysia* neurons. *Neuron* 49: 349–356, 2006.

MacAskill AF, Kittler JT. Control of mitochondrial transport and localization in neurons. *Trends Cell Biol* 20: 102–112, 2010.

Magoski NS, Kaczmarek LK. Association/dissociation of a channel-kinase complex underlies state-dependent modulation. *J Neurosci* 25: 8037–8047, 2005.

Makani S, Chesler M. Rapid rise of extracellular pH evoked by neural activity is generated by the plasma membrane calcium ATPase. *J Neurophysiol* 103: 667–676, 2010.

Mallilankaraman K, Cardenas C, Doonan PJ, Chandramoorthy HC, Irrinki KM, Golenar T, Csordas G, Madireddi P, Yang J, Muller M, Miller R, Kolesar JE, Molgo J, Kaufman B, Hajnoczky G, Foskett JK, Madesh M. MCUR1 is an essential component of mitochondrial Ca^{2+} uptake that regulates cellular metabolism. *Nat Cell Biol* 14: 1336–1343, 2012.

McDonough SI, Cseresnyes Z, Schneider MF. Origin sites of calcium release and calcium oscillations in frog sympathetic neurons. *J Neurosci* 20: 9059–9070, 2000.

Meissner G. Ryanodine activation and inhibition of the Ca^{2+} release channel of sarcoplasmic reticulum. *J Biol Chem* 261: 6300–6306, 1985.

Michel S, Wayne NL. Neurohormone secretion persists after post-afterdischarge membrane depolarization and cytosolic calcium elevation in peptidergic neurons in intact nervous tissue. *J Neurosci* 22: 9063–9069, 2002.

Munro S, Pelham HR. A C-terminal signal prevents secretion of luminal ER proteins. *Cell* 48: 899–907, 1987.

Naraghi M. T-jump study of calcium binding kinetics of calcium chelators. *Cell Calcium* 22: 255–268, 1997.

Niggli V, Sigel E, Carafoli E. The purified Ca^{2+} pump of human erythrocyte membranes catalyzes an electroneutral Ca^{2+}-H^+ exchange in reconstituted liposomal systems. *J Biol Chem* 257: 2350–2356, 1982.

Nowycky MC, Pinter MJ. Time courses of calcium and calcium-bound buffers following calcium influx in a model cell. *Biophys J* 64: 77–91, 1993.

O'Sullivan NC, Jahn TR, Reid E, O'Kane CJ. Reticulon-like-1, the *Drosophila* orthologue of the hereditary spastic paraplegia gene reticulon 2, is required for organization of endoplasmic reticulum and of distal motor axons. *Hum Mol Genet* 21: 3356–3365, 2012.

Palty R, Hershfinkel M, Sekler I. Molecular identity and functional properties of the mitochondrial Na^+/Ca^{2+} exchanger. *J Biol Chem* 287: 31650–31657, 2012.

Palty R, Silverman WF, Hershfinkel M, Caporale T, Sensi SL, Parnis J, Nolte C, Fishman D, Shoshan-Barmatz V, Herrmann S, Khananshvili D, Sekler I. NCLX is an essential component of mitochondrial Na^+/Ca^{2+} exchange. *Proc Natl Acad Sci USA* 107: 436–441, 2010.

Partridge LD, Valenzuela CF. Ca^{2+} store-dependent potentiation of Ca^{2+}-activated non-selective cation channels in rat hippocampal neurones in vitro. *J Physiol* 521: 617–627, 1999.

Patron M, Checchetto V, Raffaello A, Teardo E, Vecellio RD, Reane D, Mantoan M, Granatiero V, Szabo I, De Stefani D, Rizzuto R. MICU1 and MICU2 finely tune the mitochondrial Ca^{2+} uniporter by exerting opposite effects on MCU activity. *Mol Cell* 53: 726–737, 2014.

Perocchi F, Gohil VM, Girgis HS, Bao XR, McCombs JE, Palmer AE, Mootha VK. MICU1 encodes a mitochondrial EF hand protein required for Ca^{2+} uptake. *Nature* 467: 291–296, 2010.

Pierrot N, Tyteca D, D'auria L, Dewachter I, Gailly P, Hendrickx A, Tasiaux B, Haylani LE, Muls N, N'kuli F, Laquerriere A, Demoulin JB, Campion D, Brion JP, Courtoy PJ, Kienlen-Campard P, Octave JN. Amyloid precursor protein controls cholesterol turnover needed for neuronal activity. *EMBO Mol Med* 5: 608–625, 2013.

Pinsker HM, Dudek FE. Bag cell control of egg laying in freely behaving *Aplysia*. *Science* 197: 490–493, 1977.

Pivovarova NB, Hongpaisan J, Andrews SB, Friel DD. Depolarization-induced mitochondrial Ca^{2+} accumulation in sympathetic neurons: spatial and temporal characteristics. *J Neurosci* 19: 6372–6384, 1999.

Richter TA, Kolaj M, Renaud LP. Low voltage-activated Ca^{2+} channels are coupled to Ca^{2+}-induced Ca^{2+} release in rat thalamic midline neurons. *J Neurosci* 25: 8267–8271, 2005.

Rizzuto R, Pinton P, Carrington W, Fay FS, Fogarty KE, Lifshitz LM, Tuft RA, Pozzan T. Close contacts with the endoplasmic reticulum as determinants of mitochondrial Ca^{2+} responses. *Science* 280: 1763–1766, 1998.

Santo-Domingo J, Demaurex N. Calcium uptake mechanisms of mitochondria. *Biochim Biophys Acta* 1797: 907–912, 2010.

Seidler NW, Jona I, Vegh M, Martonosi A. Cyclopiazonic acid is a specific inhibitor of the Ca^{2+}-ATPase of sarcoplasmic reticulum. *J Biol Chem* 264: 17816–17823, 1989.

Shmigol A, Eisner DA, Wray S. Carboxyeosin decreases the rate of decay of the $[Ca^{2+}]_i$ transient in uterine smooth muscle cells isolated from pregnant rats. *Pflügers Arch* 437: 158–160, 1998.

Shmigol A, Verkhratsky A, Isenberg G. Calcium-induced calcium release in rat sensory neurons. *J Physiol* 489: 627–636, 1995.

Shutov LP, Kim MS, Houlihan PR, Medvedeva YV, Usachev YM. Mitochondria and plasma membrane Ca^{2+}-ATPase control presynaptic Ca^{2+} clearance in capsaicin-sensitive rat sensory neurons. *J Physiol* 591: 2443–2462, 2013.

Tam AK, Gardam KE, Lamb S, Kachoei BA, Magoski NS. Role for protein kinase C in controlling *Aplysia* bag cell neuron excitability. *Neuroscience* 179: 41–55, 2011.

Tam AK, Geiger JE, Hung AY, Groten CJ, Magoski NS. Persistent Ca^{2+} current contributes to a prolonged depolarization in *Aplysia* bag cell neurons. *J Neurophysiol* 102: 3753–3765, 2009.

Tang Y, Zucker RS. Mitochondrial involvement in post-tetanic potentiation of synaptic transmission. *Neuron* 18: 483–491, 1997.

Thomas RC. The Ca^{2+}:H^+ coupling ratio of the plasma membrane calcium ATPase in neurones is little sensitive to changes in external or internal pH. *Cell Calcium* 49: 357–364, 2011.

Usachev YM, DeMarco SJ, Campbell C, Strehler EE, Thayer SA. Bradykinin and ATP accelerate Ca^{2+} efflux from rat sensory neurons via protein kinase C and the plasma membrane Ca^{2+} pump isoform 4. *Neuron* 33: 113–122, 2002.

Usachev YM, Thayer SA. All-or-none Ca^{2+} release from intracellular stores triggered by Ca^{2+} influx through voltage-gated Ca^{2+} channels in rat sensory neurons. *J Neurosci* 17: 7404–7414, 1997.

Veiga-da-Cunha M, Tyteca D, Stroobant V, Courtoy PJ, Opperdoes FR, Van SE. Molecular identification of NAT8 as the enzyme that acetylates cysteine S-conjugates to mercapturic acids. *J Biol Chem* 285: 18888–18898, 2010.

Verkhratsky A. Physiology and pathophysiology of the calcium store in the endoplasmic reticulum of neurons. *Physiol Rev* 85: 201–279, 2005.

Wang KK, Villalobo A, Roufogalis BD. The plasma membrane calcium pump: a multiregulated transporter. *Trends Cell Biol* 2: 46–52, 1992.

Wayne NL, Kim J, Lee E. Prolonged hormone secretion from neuroendocrine cells of *Aplysia* is independent of extracellular calcium. *J Neuroendocrinol* 10: 529–537, 1998.

Wayne NL, Lee W, Kim YJ. Persistent activation of calcium-activated and calcium-independent protein kinase C in response to electrical afterdischarge from peptidergic neurons of *Aplysia*. *Brain Res* 834: 211–213, 1999.

Werth JL, Thayer SA. Mitochondria buffer physiological calcium loads in cultured dorsal root ganglion neurons. *J Neurosci* 14: 348–356, 1994.

Wheeler DG, Groth RD, Ma H, Barrett CF, Owen SF, Safa P, Tsien RW. Ca_V1 and Ca_V2 channels engage distinct modes of Ca^{2+} signaling to control CREB-dependent gene expression. *Cell* 149: 1112–1124, 2012.

White BH, Kaczmarek LK. Identification of a vesicular pool of calcium channels in the bag cell neurons of *Aplysia californica*. *J Neurosci* 17: 1582–1595, 1997.

Wilson GF, Richardson FC, Fisher TE, Olivera BM, Kaczmarek LK. Identification and characterization of a Ca^{2+}-sensitive nonspecific cation channel underlying prolonged repetitive firing in *Aplysia* neurons. *J Neurosci* 16: 3661–3671, 1996.

Wingrove DE, Gunter TE. Kinetics of mitochondrial calcium transport. II. A kinetic description of the sodium-dependent calcium efflux mechanism of liver mitochondria and inhibition by ruthenium red and by tetraphenylphosphonium. *J Biol Chem* 261: 15166–15171, 1986.

Zacharias DA, Strehler EE. Change in plasma membrane Ca^{2+}-ATPase splice-variant expression in response to a rise in intracellular Ca^{2+}. *Curr Biol* 6: 1642–1652, 1996.

Zenisek D, Matthews G. The role of mitochondria in presynaptic calcium handling at a ribbon synapse. *Neuron* 25: 229–237, 2000.

Zhang XF, Forscher P. Rac1 modulates stimulus-evoked Ca^{2+} release in neuronal growth cones via parallel effects on microtubule/endoplasmic reticulum dynamics and reactive oxygen species production. *Mol Biol Cell* 20: 3700–3712, 2009.

Zhou W, Jones SW. The effects of external pH on calcium channel currents in bullfrog sympathetic neurons. *Biophys J* 70: 1326–1334, 1996.